SPECTROSCOPIC EXAMINATION OF CARBON DIOXIDE LASER PRODUCED GAS BREAKDOWN

Robert William Stevenson

NAVAL POSTGRADUATE SCHOOL
Monterey, California

THESIS

SPECTROSCOPIC EXAMINATION
OF CARBON DIOXIDE LASER
PRODUCED GAS BREAKDOWN

by

Robert William Stevenson

June 1975

Thesis Advisor: A.W. Cooper

Approved for public release; distribution unlimited.

REPORT DOCUMENTATION PAGE		READ INSTRUCTIONS BEFORE COMPLETING FORM
1. REPORT NUMBER	2. GOVT ACCESSION NO.	3. RECIPIENT'S CATALOG NUMBER
4. TITLE (and Subtitle) Spectroscopic Examination of Carbon Dioxide Laser Produced Gas Breakdown		5. TYPE OF REPORT & PERIOD COVERED Master's Thesis; June 1975 6. PERFORMING ORG. REPORT NUMBER
7. AUTHOR(s) Robert William Stevenson		8. CONTRACT OR GRANT NUMBER(s)
9. PERFORMING ORGANIZATION NAME AND ADDRESS Naval Postgraduate School Monterey, California 93940		10. PROGRAM ELEMENT, PROJECT, TASK AREA & WORK UNIT NUMBERS
11. CONTROLLING OFFICE NAME AND ADDRESS Naval Postgraduate School Monterey, California 93940		12. REPORT DATE June 1975 13. NUMBER OF PAGES 94
14. MONITORING AGENCY NAME & ADDRESS(if different from Controlling Office)		15. SECURITY CLASS. (of this report) Unclassified 15a. DECLASSIFICATION/DOWNGRADING SCHEDULE

16. DISTRIBUTION STATEMENT (of this Report)

Approved for public release; distribution unlimited.

17. DISTRIBUTION STATEMENT (of the abstract entered in Block 20, if different from Report)

18. SUPPLEMENTARY NOTES

19. KEY WORDS (Continue on reverse side if necessary and identify by block number)

Carbon Dioxide Laser
Gas Breakdown

20. ABSTRACT (Continue on reverse side if necessary and identify by block number)

Light from an atmospheric pressure, double-discharge CO_2 laser, with a pulse length of 250 nanoseconds and energies from 0.7 to 2.5 joules, was focused in monatomic and diatomic gases at pressures from 1.0 to 8.0 atmospheres in order to produce a plasma for examination. The gases under investigation were Ar, He and N_2. Properties of the plasma were determined

(20. ABSTRACT Continued)

through analysis of photographs and spectroscopic measurements. Emission spectra in the visible range observed for all gases consisted of an early, intense continuum followed by a lesser continuum superimposed with strong and medium strength lines due to neutral and ionized atoms. Among the more structured lines observed were the argon II lines at wavelengths of 4545Å, 4610Å, 4765Å, 4806Å and 4880Å. The early continuum lasted for less than 0.5 microseconds, and its appearance coincided with the arrival of the laser beam in the gas chamber. The intensity of the lines varied with wavelength, and rose to maximum intensity at times ranging from 1.6 to 2.2 microseconds after the initial continuum had begun to subside. A method for predicting plasma electron temperatures was also presented. Results support theories and data on the mechanisms of breakdown published in the current literature.

Spectroscopic Examination of Carbon Dioxide Laser Produced Gas Breakdown

by

Robert William Stevenson
Lieutenant, United States Navy
B.S., Miami University, 1967

Submitted in partial fulfillment of the requirements for the degree of

MASTER OF SCIENCE IN PHYSICS

from the

NAVAL POSTGRADUATE SCHOOL
June 1975

ABSTRACT

Light from an atmospheric pressure, double-discharge CO_2 laser, with a pulse length of 250 nanoseconds and energies from 0.7 to 2.5 joules, was focused in monatomic and diatomic gases at pressures from 1.0 to 8.0 atmospheres in order to produce a plasma for examination. The gases under investigation were Ar, He and N_2. Properties of the plasma were determined through analysis of photographs and spectroscopic measurements. Emission spectra in the visible range observed for all gases consisted of an early, intense continuum followed by a lesser continuum superimposed with strong and medium strength lines due to neutral and ionized atoms. Among the more structured lines observed were the argon II lines at wavelengths of 4545Å, 4610Å, 4765Å, 4806Å and 4880Å. The early continuum lasted for less than 0.5 microseconds, and its appearance coincided with the arrival of the laser beam in the gas chamber. The intensity of the lines varied with wavelength, and rose to maximum intensity at times ranging from 1.6 to 2.2 microseconds after the initial continuum had begun to subside. A method for predicting plasma electron temperatures was also presented. Results support theories and data on the mechanisms of breakdown published in the current literature.

TABLE OF CONTENTS

LIST OF ILLUSTRATIONS

ACKNOWLEDGMENT

I wish to thank Mr. Hal Herreman for assisting in the preparation of equipment and in the conduct of the experiments. I would also like to thank Professor Kalmbach and Professor Kelly for their assistance in the spectroscopic interpretation of the data. I extend my sincere gratitude to Professor Cooper for his guidance, helpful comments and assistance in data interpretation, and to Professor Schwirzke who also assisted during the final stages of this work.

This research was supported in part by the Office of Naval Research and by the Naval Postgraduate School Foundation Research Program.

I. INTRODUCTION

The interaction of high energy laser radiation with a gas is of considerable interest in the fields of plasma production or maintenance and laser weapon or communication systems. At times it is desirable to produce or interact with a plasma, such as in heating a plasma to thermonuclear temperatures for energy production through fusion. Alternatively, if the intent is to pass a high power beam over long distances, the production of a plasma by the beam would be counterproductive. There has been considerable work done on the interaction of high intensity pulsed laser beams with gaseous and solid targets since the introduction of the ruby and neodymium lasers. The theoretical research progressed while advances in design were reducing their high cost and improving their low efficiency operating conditions. The CO_2 TEA lasers were developed to provide an inexpensive, efficient alternative to the ruby and neodymium lasers.

Prior to becoming operational, the high powered laser beam's characteristics of interaction with matter must be understood. Thus, studies of both laser and plasma characteristics have been conducted. Plasma studies have been hampered by an inability to contain the plasma long enough for adequate investigation; however, it has been determined that

instabilities can be minimized by utilizing specially constructed magnetic bottles to contain the plasma. It has also been shown experimentally and theoretically that for frequencies below the plasma cutoff frequency incident radiation will not propagate through a plasma, but will be reflected and absorbed. Even for higher frequencies a highly ionized gas will produce severe attenuation, with the absorption occurring mostly in the vicinity of the critical density. The area of most intense research at this time is in determining the mechanisms by which energy from the laser beam is coupled to the plasma, thereby increasing the plasma temperature. The CO_2 radiation at 10.6 micrometers is of great interest, since the efficiency, pulse lengths (10-100μ sec) and pulse energies (10^3-10^4 J) available at present can provide significant heating of dense plasma pinches (10^{17}-10^{18} ions per cm^3). Laser light absorption is commonly assumed to be by inverse Bremsstrahlung, with some possible anomalous mechanisms.

The investigation of a hot, dense plasma can be carried out by inducing breakdown of a gas within the confines of a pressure cell through focusing of a laser beam. The purpose of this study was to investigate the breakdown of various common gases using pulsed CO_2 laser radiation. Gases involved were argon, nitrogen and helium. Radiation from the breakdown plasma in the visible portion of the electromagnetic spectrum, with wavelengths from 4000 to 6000

angstroms, was investigated to determine its source, and the manner in which individual lines changed as breakdown progressed. Photographs of the plasma expansion were obtained to compare with oscilloscope photographs of the temporal distribution of intensity. Analysis of the data led to a model of the breakdown which supports models proposed by other workers and which have been presented in the current literature.

II. THEORY

A. GAS BREAKDOWN MECHANISMS

The entire process of plasma production whereby a gas is transformed into a highly conducting plasma may be considered to consist of four stages: initiation, growth, steady state and extinction. The mechanisms by which energy is transferred from a laser beam to the plasma are the subject of intensive research at the present time. In the initial, or formative, stage the laser radiation is producing electron-ion pairs. As the process accelerates, more pairs are formed until a steady state density is reached. At this point the energy is being passed to the plasma by inverse Bremsstrahlung and other mechanisms such as wave-wave coupling, and all incoming radiant energy in excess of the losses goes into heating. The final stage begins as the laser pulse power drops below that required to balance losses, and ionization begins to decrease as recombination increases. Each of these periods in the life of the plasma has its own distinct characteristics, which yield information on conditions within the plasma.

Detailed studies of the breakdown threshold as a function of laser peak power, laser total energy, pressure of the gas and whether or not the gas had previously been a plasma have shown that the presence of a few free electrons can

produce the greatest change in threshold. Thus, it has been determined that the controlling factor in the production of a plasma is the production of the first few (on the order of 10) free electrons. For laser radiation at 10.6 micrometers, the photon energy E = hf is only 0.117 eV. In contrast, the ionization energy for a neutral argon atom is 15.76 eV. The search for the link between these two values has taken various directions. It is now accepted by most researchers that the first few electrons are produced by multiphoton absorption. This is the simultaneous absorption of a number of quanta from the intense radiation field by a single electron. This total energy is sufficient to liberate it from the parent atom.

Once a few free electrons are present, the growth stage begins. The electrons gain energy from the electromagnetic field produced by the laser pulse between elastic collisions with neutral atoms. If the pulse power is sufficiently high, an electron can gain enough energy between collisions to ionize an atom, creating two low energy electrons. This process continues as a cascade until one of two possibilities occurs: The laser radiation stops, or complete ionization to the degree permitted by the laser energy is attained. If the laser pulse continues, the plasma is heated to a point where all the incoming energy is dissipated by various mechanisms, producing a steady state situation. This second possibility is the desired operating condition for laser

heating of a plasma to thermonuclear temperatures. Additional mechanisms that might assist in the production of electrons, but are not of sufficient interest to warrant serious consideration or detailed study here, are direct stripping of electrons from atoms by the laser radiation electric field, and tunneling of an electron through its potential barrier under the influence of a high frequency field. Multiphoton absorption cannot account for the great avalanche of electron-ion pairs produced, and so is ignored as a growth mechanism.

The formative, or growth, stage of plasma development consists of the amplification of the number of electron-ion pairs until the state of "breakdown" is reached. Breakdown is defined as attainment of a degree of fractional ionization sufficient to cause significant absorption and scattering of the laser radiation. Practically, this means an electron density of about 10^{13} cm^{-3} in the focal region is required. At this point the optical electric field is sufficient to support continued growth. The avalanche growth of ionization is maintained through absorption of energy from the field. The absorption process may be considered either as an extension of microwave breakdown theory or as inverse Bremsstrahlung (free-free transition with absorption of a photon by an electron occurring in the presence of an ion). At this stage the plasma wave modes are not yet established, and wave-wave coupling may be ignored. The combined duration

of initiation and growth stages is only a few nanoseconds. This is short with respect to the laser pulse length, leaving a great deal of time for heating to occur by inverse Bremsstrahlung and wave-wave energy coupling. Simultaneously with breakdown a bright flash of blue-white light and an audible crack occur. Figure 1 shows a typical "spark", as photographed with an open face camera.

The extinction phase begins when the laser pulse power drops to a level which is insufficient to maintain the plasma density. Loss mechanisms such as recombination and radiation dominate during this phase. The density drops off exponentially, and the time to complete extinction is several orders of magnitude greater than the growth time. Studies of the afterglow (Section V) show measurable effects as long as 7 microseconds after initiation of the plasma. During this period the plasma expands and cools as a result of radiation emission, diffusion, electron attachment and recombination.

B. CASCADE DEVELOPMENT OF GROWTH STAGE

The mechanisms by which energy from a laser beam can produce ionization and support plasma growth through breakdown are incompletely known. Contributing to the problem are the reported results obtained by numerous workers in the field. Even with similar experimental conditions, many different plasma parameter values have been obtained, leading

to unresolved conflicts. The difficulties inherent in obtaining precise measurements of conditions within a plasma which lasts only a few microseconds are most probably at fault. In addition, each research effort involved conditions which varied slightly from other efforts. Even within a range of experiments of a similar nature, such diverse but prevalent problems as imprecise definition of the focal region, inaccurate knowledge of the variation in radiation within this volume, uncertainties in the radiation power density and in the angular divergence of the laser beam resulted in a wide spectrum of results. Nevertheless, out of this assortment of information has come sufficient evidence to support the view that the growth stage proceeds as a result of a collisional cascade fed by energy absorbed in the inverse Bremsstrahlung process. This is classically equivalent to excitation and ionization through electron-ion collisions in which the interaction energy is drawn from the electromagnetic field of the light wave. This concept is essentially an extrapolation of microwave discharge theory to optical frequencies.

Thus, once liberated in the focal region during the early stage of the laser pulse by multiphoton absorption, free electrons gain thermal energy from the electromagnetic field. When their energies exceed the atomic ionization potential they cause amplification of the electron-ion concentration through collision ionization. Simultaneously

there occurs a loss of free electrons from the focal region due to diffusion, recombination and attachment. If the rate of production exceeds the loss rate, the concentration increases and breakdown occurs.

A formal discussion of breakdown must begin with the continuity equation for electron density:

$$\frac{\partial n}{\partial t} = \left(\nu_i - \nu_a\right) n + D\nabla^2 n - \alpha_R n^2 \qquad (1)$$

where ν_i is the ionization rate, ν_a is the attachment rate, D is the electron diffusion constant and α_R is the recombination coefficient. Recombination losses are usually not important in the early stage of plasma development, and will be neglected. The focal volume can be approximated by a cylinder of radius r and length l, where $l > r$. Assuming a constant ionization rate inside and zero electron density outside the cylinder, equation (1) can be solved to yield

$$n_f = n_o \exp\left[\left(\nu_i - \nu_a - D/L_D^2\right) T\right] \qquad (2)$$

where $L_D = r/2.405$ is the diffusion length, T is the laser pulse length, and n_f and n_o are the final and initial electron densities, respectively.

For the gas to break down, a certain electron density must be reached before the end of the laser pulse. The criterion is represented by a number k_{cr}, defined so that

the number of electrons generated in a time T by a free electron is $2^{k_{cr}}$. k_{cr} is usually taken to be 43, corresponding to a multiplication factor of 10^{13} for each free electron initially present. By rearrangement of equation (2)

$$\nu_i = D/L_D^2 + \nu_a + \left(K_{cr}/T\right) \ln 2 \tag{3}$$

which, in terms of the net rate at which electrons gain energy, $d\epsilon/dt$, and the ionization potential of the gas, I, can be written as

$$\nu_i = \frac{\ln 2}{I} \cdot \frac{d\epsilon}{dt} \tag{4}$$

According to microwave theory, electrons gain thermal energy from the radiation field by elastic collisions with neutral atoms at a rate

$$\left.\frac{d\epsilon}{dt}\right|_{gain} = \frac{e^2 E^2}{m} \cdot \frac{\nu_c}{\omega^2 + \nu_c^2} \tag{5}$$

where E is the rms electric field, m is the electron mass, ω is the angular frequency of the radiation, and ν_c is the electron-atom collision frequency. At the same time, electrons lose energy in both elastic and inelastic collisions. The average energy loss due to elastic collisions is

$$\left.\frac{d\epsilon}{dt}\right)_{\text{elastic loss}} = -\frac{2m}{M}\langle\epsilon\rangle\nu_c \tag{6}$$

where M is the atomic mass and $\langle\epsilon\rangle$ is the average electron energy. In an inelastic collision there is a change in the internal state of the atom at the expense of the electron's kinetic energy. An exact calculation of such a loss term is difficult because atoms and molecules have many levels to which they may be excited, which would prevent a determination of the average loss per collision. Reabsorption of radiation from one atom by a neighboring atom may also occur. This phenomenon is known as resonance radiation trapping. Energy can also be lost by various means whereby it passes out of the focal volume. Rather than make an unreliable calculation of the energy loss term through inelastic collisions, two characteristic parameters are used to provide a workable equation. The loss rate must be proportional to the production rate of excited atoms. Then energy may be lost in two possible ways: (i) loss independent of focal volume, or (ii) loss dependent on focal volume with an L_D^{-2} dependence. Combining these losses, the inelastic collision energy loss may be written

$$\left.\frac{d\epsilon}{dt}\right)_{\text{inelastic loss}} = -\frac{I}{\ln 2}\left(\alpha + \frac{\beta}{L_0^2}\right)\nu_c \tag{7}$$

where α and β are the two characteristic parameters. The quantity in parentheses is dimensionless. The factor I/ln2 introduced in equation (7) serves in simplification of the final result. Combining equations (3) through (7), and defining the power threshold density as $P_{th} = (c/4\pi)E^2$, the following form for the breakdown threshold power density is found:

$$P_{th} = \frac{cmI}{4\pi e^2 \ln 2} \cdot \frac{\omega^2 + \nu_c^2}{\nu_c} \left[\frac{\kappa_{cr}}{T} \ln 2 + \frac{D}{L_D^2} + \nu_a \right.$$

$$\left. + \frac{2m\langle\epsilon\rangle \ln 2}{MI} \nu_c + \left(\alpha + \frac{\beta}{L_D^2} \right) \nu_c \right] \qquad (8)$$

The dependence of threshold on many experimental parameters has been extensively investigated and reported. The values for threshold power are either read from graphs [Refs. 3, 28] or determined independently by experimentation with the system at hand.

C. EXPANSION OF THE PLASMA

Several models have been proposed to account for the manner in which the plasma expands from the initial focal volume. No one theory is sufficient to account for the complete process. Among the theories finding greatest acceptance are a radiation supported detonation wave, a blast wave, a breakdown wave, a radiation transport wave or a travelling ionization wave. The most promising explanation

is that of a radiation supported detonation wave during the time the laser pulse is supplying energy, and a blast wave during the later stage.

Growth of the plasma is predominantly in the direction opposite to the laser light flux. This phenomena can be adequately described by considering the expansion as a radiation supported detonation wave. The theory for this model is quite detailed, and beyond the scope of this overview. However, in brief, the theory considers energy absorbed by the plasma from the laser beam to be the driving force for the wave front. The moving wave is considered as a shock, and requires thermo- and gas dynamic methods to determine conditions in the vicinity of the wave. Wave propagation velocity is found to depend on the specific heat ratio behind the wave, on the laser irradiance and on the ambient density in front of the wave:

$$V = \left[2\left(\gamma^2 - 1\right) G_o / \rho\right]^{1/3} \qquad (9)$$

A detailed study of this phenomenon was conducted by Zel'dovich and Raizer and the results appear in Ref. 33. Experimental verification of the dependence of wave speed on the 1/3 power of laser irradiance has been obtained by Mandel'shtam [Ref. 20], which lends credence to this theory.

When the laser irradiance has dropped below the level required for LSD wave propagation, a new theory must be

developed to explain the continued expansion of the plasma shock front. This is not to be confused with the expected diffusion into 4π steradians which also occurs as the plasma cools. Rather, this is a measurable shock wave. It can satisfactorily be explained as a blast wave, which requires energy only in its production stage. Once propagating, a blast wave needs no further input of energy. The expansion velocity decreases from that of the LSD wave.

Photographs of the luminous front of an expanding, laser produced plasma have been obtained by numerous workers using both streak and high speed framing cameras as well as with shadowgraphs. Such a photograph appears in Fig. 9. The position of the plasma has been shown by Daiber and Thompson [Ref. 7] to have a 0.6 power time dependence in the presence of the laser pulse, and a 0.4 power dependence in the afterglow. This is strong evidence in support of the existence of multiple mechanisms in the expansion phase.

D. RADIATION FROM THE PLASMA

Radiation has been observed from breakdown plasmas in the visible, ultraviolet and soft x-ray regions of the electromagnetic spectrum. The visible light is extremely intense, of a bluish-white color, and is radiated more or less uniformly into 4π steradians. Lampis and Brown [Ref. 18] report that during the period in which the laser pulse is producing ionization and heating the plasma to a high temperature, an intense continuum is emitted. The plasma

then begins expanding into 4π steradians as it cools and diffuses. Later, individual lines are radiated, and this radiation persists for several microseconds. Observations of the continua and lines have been made by Evtushenko [Ref. 9], who reports that the lines from more highly ionized states appear earlier than the neutral lines.

A variation in the time of line appearance would be expected for plasmas with local thermodynamic equilibrium. If the electron-atom and electron-ion collision rate is sufficiently high, the temperature of the electrons would control the excitation rates. In the absence of local thermodynamic equilibrium (LTE), emission would occur during radiative decay from the recombination levels, which would not necessarily be those with the highest energy levels. This would result in a more even distribution of line radiation times. Thus, based on observations, it must be assumed that LTE exists in the plasma, and that as the plasma expands and cools the lines arising from the highest energy levels would appear first.

The accepted theoretical model considers the radiation to arise from Bremsstrahlung as well as recombination and radiative decay. This produces a continuum underlying the line spectrum. One important result of this observed continuum is that temperatures within the plasma can be determined by spectroscopic methods, as outlined by Griem [Ref. 11].

The usual methods of determining temperature include line-to-continuum ratios and line-to-line ratios of intensity. Obtaining the temperature from the ratio can be accomplished by use of an equation pertinent to the method employed, but can also be estimated from graphs produced for frequently observed gaseous elements. Griem [Ref. 11] is considered to have compiled the most complete information on extracting temperature information from spectroscopic data. Temperatures calculated for the laser produced plasmas in laboratory experiments have ranged from 1 to 300 eV, depending on the method of determination and the experimental conditions.

In addition to temperature, the electron density can be obtained through measurements of Stark broadening. For high densities the Stark effect yields the major contribution to line width. The electron density n_e is related to the full Stark width $\Delta\lambda_s$ by

$$n_e = C(n_e, T)\,\Delta\lambda_s^{3/2} \tag{10}$$

where the coefficient $C(n_e,T)$ is only weakly dependent on electron density, and is tabulated by Griem [Ref. 11] for many lines. Observations by many workers indicate a very dense plasma is produced initially, consistent with complete single ionization of the gas within the focal volume when appropriate pressure and laser energy requirements are met.

In the afterglow the density drops to about 1/10 of the maximum density reached and persists for at least a microsecond [Ref. 4].

E. SCATTERING OF LASER RADIATION

Numerous intermingled effects are present in a plasma due to both random and forced motion of ions and electrons. This motion can be analyzed to determine the velocity distribution in any direction, the natural plasma oscillation frequencies, as well as to yield information on the collisions taking place in the plasma. The plasma effects are felt as perturbations on an incident electromagnetic wave. The success of such determinations depends on many factors, not the least of which is that the incident radiation not perturb the plasma conditions. Since calculations show that scattered radiation can be detected only for extremely high input intensities, this requirement becomes significant when the fine structure of the plasma is to be investigated.

Scattering occurs when incident light strikes a nonuniformity in a medium. For purposes of this discussion the nonuniformity is produced by electron and ion density fluctuations in the plasma, and the incident light is a high intensity laser beam. The density fluctuations are the result of natural oscillations from thermal motion or wave action.

According to Kunze [Ref. 17], fluctuations stochastic in nature are associated with uncorrelated density fluctuations,

and are attributed to electron (or ion) thermal motion. Those dependent on long range electrical forces are associated with collective (wave) phenomena. Since the scattered radiation field is proportional to velocity divided by mass, the direct ion contribution is negligible. Ions shielded by electrons do provide a major portion of scattering in the highly correlated range.

The following discussion on scattering was extracted from Ref. 17, in which Kunze explains in detail the various effects which may be examined through measurements of scattered radiation.

The scattered spectrum consists of contributions from several sources, but the predominant feature is a doppler shift from the incident frequency. Doppler effects can be shown to depend, not on the direction of observation, but on the electron velocity component in the direction of $\vec{k}$ - defined as

$$\vec{K} = \vec{K}_s - \vec{K}_o \qquad (11)$$

where $\vec{k}_s$ is in the scattered (observed) direction and $\vec{k}_o$ is in the direction of incident light, while the magnitude of each is equal to 2π divided by the respective wavelength. The frequency shift of the scattered radiation (for $k_o \approx k_s$) is

$$\Delta\omega = \omega_o - \omega_s \approx \left(\vec{K}_s - \vec{K}_o\right) \cdot \vec{V} = \vec{K} \cdot \vec{V} \tag{12}$$

If thermal effects predominate, the spectrum has a half width proportional to $\sqrt{T_e}$, with T_e as the electron temperature, and appears Gaussian for a Maxwellian velocity distribution. If wave effects are present, the spectrum becomes distorted, and a doublet appears at

$$\omega = \omega_o \pm \sqrt{\omega_{pe}^2 + \frac{3K_B T_e K^2}{m_e}} \tag{13}$$

due to electron waves. Here ω_{pe} is the electron plasma frequency, K_B is the Boltzmann constant and m_e is the electron mass.

Thus, temperature and velocity information may be extracted through scattering measurements if a sufficient source of radiation is available. The source must have high monochromaticity. In addition, high intensity is required, because the relation between incident intensity and the number of scattered photons required for detection is such that $N_o n_e l \sim 10^{31}$ cm^{-2}, where N_o is the number of photons in the incident pulse, and l is length of the scattering volume. For a CO_2 laser at one joule, $N_o = 5.333 \times 10^{19}$. In a laboratory laser-produced plasma, l is about 0.5 cm for the fully expanded plasma. Thus, a density of only 10^{12} cm^{-3} is required. This is well below

the level required to produce breakdown (10^{13} cm^{-3}), and is therefore within the capability of present systems. For spectral information other than density, another order of magnitude is required. This is still the lower limit for breakdown, and is easily attainable. A good rule of thumb is to consider a 10MW incident pulse as producing a 1μW scattered output signal. If time resolution is unimportant, and the plasma can be investigated over a period on the order of 1ms, lower intensity can be used.

F. CALCULATIONS

The following simplistic model has been developed to provide a rough estimate type of energy balance during the energy absorption phase of plasma production. This empirical model is offered here for consideration as a method of predicting the anticipated electron temperatures in a breakdown plasma. Although an attempt has been made to keep arbitrary assumptions to a minimum, it should be noted that the stability of the results is most sensitive to the plasma expansion rate assumed. Many different rates have been measured and generally fall in the range of 1×10^7 to 5×10^7 cm/sec - but Lampis and Brown [Ref. 18] obtained 1×10^6 cm/sec. Thus, it must be emphasized that this model was produced with only one objective: to yield results that agree with previously published electron temperature values for similar conditions. More conventional

methods of prediction may accurately take into account those factors with which they deal; however, the results are far from satisfactory. Behrens [Ref. 3], in following the standard approach, reaches a conclusion that the electron temperature is 5353 eV, which is higher by a factor of 100 to 1000 than experimental results indicate [Refs. 4, 15]. Therefore, a less rigorous, but more realistic approach would seem useful for a "back of the envelope" calculation in preparation for measurements.

The laser-plasma interaction is considered here to proceed as follows: (a) The laser pulse is focused into a small focal volume, producing a large electromagnetic field; (b) A few (10) electrons are produced by multi-photon absorption; (c) Growth of the plasma proceeds by collisional ionization; (d) Growth of the plasma continues until 100% single ionization is achieved (if gas is initially at one atmosphere pressure), or to an equivalent ionization state for gases at higher pressures. During this time, that energy not absorbed is transmitted. (e) Cutoff and reflection occur when ionization has produced a plasma frequency equal to that of the incident radiation at 2.83×10^{13} Hz, and this occurs at 9.9×10^{18} cm^{-3} electron density; (f) Heating of the plasma begins, as well as ionization of a volume of un-ionized gas slightly closer to the laser; (g) The ions and electrons are heated, and the

expanding plasma moves the absorption region back up the beam. This can occur since some electrons are present, lowering the breakdown threshold, and the laser energy is reflected from the forward portion of the plasma, increasing the irradiance in the un-ionized region. (h) Ionization occurs in the moving focal region until the field drops below that required to sustain the breakdown process; (i) The ionization rate drops until recombination losses dominate, and all further laser pulse energy is considered to be utilized in heating the plasma (or is reflected); (j) After the pulse has dropped to near zero intensity, cooling of the plasma proceeds exponentially, with the plasma expanding more or less uniformly into 4π steradians.

This method of describing the process follows from consideration of the development as a breakdown wave as theorized by Raizer [Ref. 27], although it could equally well be considered as an LSD wave. Determination of the total volume to be ionized is made by assuming an expansion rate within the confines of the geometrical laser beam cone.

1. Absorption of Laser Radiation and Electron Temperature

The basic assumption in the method presented here is absorption of the laser energy by the entire volume of ionized gas. This is valid only if the calculated volume is consistent with all previously established parameters. The volume assumed here is that of a narrow pyramid, with the original focal point as the apex, and the final expansion

point as the base. The original focal volume is too small to be considered here, as is the diameter of the focal spot. The errors introduced are small in comparison to those produced by small changes in the expansion rate assumed. The point in the laser pulse at which cutoff of the transmission occurs is taken as the level of field intensity required to support breakdown, although the actual point is somewhat lower. In attempting to find the appropriate length of time for ionization, it was found that the expansion rate and time were mutually dependent if a believable result was to be obtained. It was determined that good values could be calculated if the product of ionization time and expansion velocity fell in a small range about 0.15 cm. This was consistent with photographs of the plasma, but no acceptable theory could be produced to justify such an assumption. Nevertheless, since the only concern was to produce reasonably accurate electron temperatures, calculations were made based on an expansion rate of 1×10^6 cm/sec, with the ionization time equal to 150 nanoseconds.

If absorption is considered to proceed by inverse Bremsstrahlung, the expression developed by Offenberger [Ref. 23] for the effective energy absorption coefficient in Beer's law,

$$W = W_o\left(1 - e^{-KL}\right) \tag{14}$$

can be utilized for determination of the absorption length. Here W is the laser energy absorbed in a distance L from a point where the energy is W_o for a medium with absorption coefficient K. Behrens [Ref. 3] determined by measurements of transmission through the plasma that W/W_o was about 74%. The expression for K is given as

$$K = 1.8 \times 10^{-35} \left(n_e^2 / T_e^{3/2} \right) \quad cm^{-1} \tag{15}$$

If the electron density is assumed as that at which the plasma frequency equals the laser frequency, and the electron temperature is taken as 65 eV (a typical value as calculated by Raizer [Ref. 26]), then the value of K is 3.37 cm^{-1}. Both this value and the 74% absorption were inserted into equation (14), which was solved to yield an interaction length of 0.4 cm. Thus, the expansion assumed in the model did not exceed the e-folding length for absorption, and the assumption of absorption within the entire volume was consistent with previously established parameters.

Determination of the focal volume proceeded by geometry from a rectangular beam size at the focusing lens to the apex of the pyramid at a distance of 2.54 cm, equal to the focal length, from the lens. From the focal point, with a 0.15 cm length (h), the base dimensions were identical to the length, which produced a base area (B) equal to 0.0225 cm^2. The total focal volume was found to be

$$V = \frac{1}{3} B h = 3.37 \times 10^{-3} \text{ cm}^3 \tag{16}$$

At one atmosphere of argon gas, considering the gas ideal and at room temperature,

$$n = p/kT = 2.45 \times 10^{19} \text{ cm}^{-3} \tag{17}$$

Thus, within the focal volume were

$$N = nV = 8.269 \times 10^{16} \text{ atoms} \tag{18}$$

The energy in the laser pulse varied from shot to shot, and was also intentionally varied. For the lowest energy pulse, 0.733 ±.037 joules passed into the gas cell. This corresponds to 4.57 x 10^{18} eV. Of this, 24% was transmitted prior to breakdown. Thus, 3.478 x 10^{18} eV were available for use. The ionization potential of neutral argon atoms is 15.76 eV. Therefore a total of 1.303 x 10^{18} eV was utilized to produce complete ionization. After the ionization energy had been subtracted from that available, there remained 2.175 x 10^{18} eV which could be utilized in heating and reflection. Experimental observations indicated that reflection was on the order of 1%. This left 2.153 x 10^{18} eV for heating. Since two particles were produced in each ionization, and 100% ionization was assumed, there were

1.654×10^{17} particles to receive the heating energy equally. Dividing the available energy by the number of particles yielded 13 eV per particle during the brief period of maximum temperature. This compares with results reported in the literature of 1 to 65 eV [Refs. 4,26]. When pulses of higher energy were used for the calculations, the temperatures scaled well. Table VII, Appendix B lists the temperatures obtained by this method for the gases and energies used in this experiment. It was determined through analysis of the spectra observed for argon that the temperature calculated here was too low to be consistent with the presence of Ar II lines if local thermodynamic equilibrium was assumed. Therefore, the actual temperature was believed to be closer to 21 eV. The calculations for nitrogen produced a similar discrepancy. The calculations for helium, however, were consistent with observations.

2. Electron Density in the Plasma

The most direct method of estimating density of electrons within the plasma would be to consider the gas to be 100% singly ionized. This would yield a value equal to the original density of the gas. However, justification would be required for such an assumption. Only if cutoff was observed, and if the plasma frequency corresponded exactly to the original density, and no indications of more highly ionized atoms were present could such a method give the correct results. Therefore, a more prudent method of

estimating the density would be to set upper and lower bounds on the density.

The electron plasma frequency is given as

$$\omega_{pe} = \left[n_e e^2 / m_e \epsilon_o \right]^{1/2} = 8.99 \times 10^3 \, n_e^{1/2} \qquad (19)$$

where n_e is the electron density in cm^{-3}, e is the elementary charge, m_e is the electron mass and ϵ_o is the permittivity of free space. When the plasma frequency is equal to or greater than the laser frequency, significant reflection and absorption of the laser energy occurs and transmission through the plasma is cut off. For the CO_2 laser the frequency is 2.83×10^{13} Hz. Since cutoff is observed, setting the plasma and laser frequencies equal yields a minimum density of 9.9×10^{18} cm^{-3}.

An upper limit can be obtained through spectroscopic measurements. Any significant number of atoms in an ionization state will radiate discernible and identifiable lines. Thus, the highest degree of ionization present in the plasma can be ascertained. If 100% ionization at all levels for which lines are present is assumed, then the maximum electron density can quickly be calculated.

In this experiment, no argon III lines were observed. Therefore, the upper bound for the density could be set at 2.45×10^{19} cm^{-3}, which is equal to the original gas density.

While not capable of the accuracy provided by other methods based on spectroscopy, an estimate of this type appears to give reasonable order of magnitude figures.

III. EQUIPMENT

A carbon dioxide (CO_2) Transverse Excitation at Atmospheric pressure (TEA) laser was used throughout the study. A description of the laser is given by Strickland [Ref. 32] and by Behrens [Ref. 3]. The laser output was focused with a germanium lens into either of two pressure chambers. The gas breakdown produced by the intense radiation field was observed spectroscopically with either a small, one meter spectrograph, or with a three meter dual monochromator built by George A. Orlicki in 1972. Energy in the laser pulse was determined with a ballistic thermopile, and the pulse shape was determined using a photon drag detector. Photographs of the breakdown were obtained with an Imacon 600 high speed framing camera, and an open face camera.

A. TEA LASER

The laser system consisted of a resonant cavity, a Tachisto Marx type generator, a pulse shaping network composed of passive electrical components, a D. C. power supply and a gas flow system. The resonant cavity consisted of a gas filled rectangular container 40 inches long, 12 inches wide, 6 inches high, constructed of 1 inch thick acrylic lucite, and two mirrors. The ends of the box each contained a NaCl crystal plate serving as a Brewster window. Inside the box was the electrode assembly, which was modified for

this study. The new anode was constructed of 3/4 inch thick aluminum, cut to fit the inside of the cavity, leaving only 1/4 inch spacing around the rounded edges. The new cathode consisted of 131 blades constructed from 1/64 inch thick aluminum, separated by 1/4 inch lucite spacers and electrically connected by two threaded brass rods. The trigger assembly consisted of 130 glass-encased nichrome wires placed between the cathode plates, with the wire set at the same height as the edge of the cathode blade, and parallel to it. This electrode configuration is depicted in Fig. 2.

Selective excitation of the CO_2 upper laser level (the 001 level) in a TEA laser is a collision dominated process. Energy is injected by an electric discharge that creates a uniform flux of electrons with average energy near one electron volt. Inelastic collisions between the accelerated electrons and the CO_2 molecules occur rapidly. Since resonances exist in the CO_2 excitation cross section for electron energies of 0.3, 0.6 and 0.9 electron volts which coincide with the vibrational ladder of energy levels, preferential excitation of the molecules occurs. Then collisions between excited and unexcited molecules populate the upper laser level very efficiently. The high efficiency arises from the fact that the energy levels are equally spaced, so little energy is lost during transitions up or down the ladder. Typical processes are:

$$CO_2\ (00\nu_3) + CO_2\ (000) \rightarrow CO_2\ (0,0,\nu_3-1) + CO_2\ (001)$$

$$CO_2\ (002) + CO_2\ (000) \rightarrow 2\ CO_2\ (001)$$

This high excitation efficiency, when coupled with a quantum efficiency of nearly 41 percent, enables one to attain an operation efficiency as high as 25 percent.

Addition of nitrogen to the gas supply provides another form of selective excitation. Electron impact excites the nitrogen molecules to upper vibrational energy levels. The vibrational levels of the nitrogen and CO_2 match closely, so an efficient transfer of energy occurs. Once again the CO_2 vibrational ladder populates the upper laser level.

As the CO_2 molecule decays, or is stimulated, from the upper to the lower laser level it emits a photon at 10.6 micrometers. It must be removed quickly from this level or the population inversion will be destroyed. This drainage is provided through collisional energy transfer. Collisions with ground state CO_2 molecules will depopulate the lower laser level, but create a bottleneck at the CO_2 (010) level. To avoid this reduction in laser cycle rate the collision rate must be increased. Use of a light gas, such as helium, with a collision rate many times that of the CO_2 will eliminate the problem.

The gas mixture used in the past with the NPS laser was 85 percent He, 7.5 percent CO_2 and 7.5 percent N_2. Preliminary investigation of the new electrode operating characteristics

indicated that an energy peak existed for a helium percentage between 87.5 and 90. For this study a 90/5/5 mixture was utilized, at a flow rate of approximately 1 cubic foot per minute.

Conditions for lasing were produced by electrical breakdown between the electrodes. This promoted the direct electron impact and molecule-molecule energy transfer resulting in the population inversion of the CO_2 levels. Atmospheric pressure operation is preferable to low pressure due to the greater molecular density, and consequently greater available energy. Transverse excitation involves production of a large discharge volume through use of a short discharge length and large area.

Large working voltages and the low impedance of a small electrode gap allow rapid injection of discharge excitation energy. Double discharge preionization techniques were used to obtain a uniform volume discharge. The new electrode system used in this study was designed to produce a greater corona, more even distribution of space charge, and to eliminate edge effects. The new gap size was 5.8 cm. Preionization was accomplished through use of insulated trigger wires maintained at ground potential, along with the anode, as the cathode was charged to a large, negative potential by the Marx generator. The placement of the trigger wires near the sharp edges of the cathode blades

produced an intense corona due to the high electric field concentration.

The electrical power for excitation of the gas was produced by a three-stage Marx generator supplied with a positive voltage up to 22 kilovolts and 15 milliamps by an unregulated D. C. power supply. With the voltage multiplication feature of the Marx, up to 66 KV could be obtained across the electrodes. To produce a uniform glow discharge for gas pumping, it was necessary to limit the discharge time. Proper operation required rapid breakdown to achieve the generation of a glow discharge, then the reduction of the voltage to prevent arc formation. Control of the voltage rise time and decay time constants of the input energy pulse from the Marx to the laser cavity electrodes was effected through the use of a pulse-shaping network of passive circuit elements consisting of resistors, inductors and capacitors. This network is described in Ref. 32.

The resonant cavity for the laser consisted of the gas filled laser box and two mirrors. The back mirror was a 4 inch diameter polished copper mirror with a three meter radius of curvature; and the front mirror was a 4.5 inch diameter plane parallel germanium mirror, which transmitted approximately 45 percent of the radiation striking it from inside the cavity. The total energy in an output pulse varied, depending on the excitation voltage used. Figure 3 is a plot of laser pulse shapes at various input voltages.

The first peak in the output pulse resulted from electron impact excitation of the CO_2, and the second was from N_2 - CO_2 inelastic collision pumping.

Some important characteristics of the laser system are listed in Table I, Appendix B.

It should be noted here that the original design for the cathode called for two support bars made of insulating material, which would prevent the trigger wires from falling out of position, to be bolted in place so as to run the full length of the cathode. During system tests, arcing occurred from the bolts to the anode. The support bars were removed and proper glow conditions were obtained up to 54 KV.

Also of concern was the fact that the glow was strongest at the end with the electrical connections, tapering off to a considerably decreased intensity at the other end. When arcing occurred, it did so at the end with the electrical connections, and it produced severe pitting of the anode. (See recommendations.)

B. PRESSURE CELLS

Two pressure cells constructed of aluminum were used to contain gases of interest in the experiment. Although capable of withstanding pressures from 0.01 to 10 atmospheres, the chambers were only operated from 0.1 to 8.0 atmospheres in this study. One of the cells was cubic, containing a volume of 255 cm^3. The other was cylindrical, with 720 cm^3

volume. This chamber permitted viewing the plasma from zero, 45, 90 and 135 degrees with respect to the laser beam axis. All windows (viewing ports) were 2 inches in diameter. The entrance and exit ports had potassium bromide windows, which transmit 93 percent from 1 to 20 micrometers; and the side windows were of Pyrex 7913 tempered glass, which is transparent to visible light. The top of both cells contained fittings for gas inlet and outlet, pressure gauge, vacuum pump and a cylindrical alumina (Al_2O_3) rod of diameter 0.635 cm which served as a reference mark inside the cell. The laser beam was focused at the center of the cell by a 2.54 cm focal length, f/1, double convex, anti-reflection coated germanium lens. Germanium was chosen for optical components in this system for several reasons: (i) It has a high thermal conductivity which allows efficient cooling and reduces the chance of damage at high power levels of operation; (ii) It has a relatively low absorption, and at 10.6 micrometers absorption is on the order of 1 percent per millimeter; (iii) It can be polished and coated to a very high quality optical finish.

Some important properties of germanium are listed in Table II, Appendix B.

C. DETECTORS

The forward scattered laser light was focused onto the entrance window of a photon drag detector, which was connected

to a Tektronix 555 oscilloscope. In this way the pulse shape of the transmitted laser pulse was determined. When integrated and set equal to the energy contained in the pulse, peak values for laser output power could be obtained. This was done graphically by Behrens [Ref. 3]. The Photon drag detector operates by transfer of momentum from incident photons to free carriers in a doped germanium crystal. This produces a voltage gradient which is proportional to the incident intensity. This voltage is amplified and appears on the oscilloscope as depicted in Fig. 3. Some specifications of the photon drag detector are given in Table III, Appendix B.

The total energy in each laser pulse can easily be obtained by directing the beam into a ballistic thermopile. In this study a portion of the beam was split off and focused into the thermopile by a copper mirror. This permitted simultaneous use and measurement of the energy in the pulse. The experimental arrangement was set up and the energy was measured at the lens focal point, then compared with that from use of the beam-splitter. In this way there was no loss of accuracy due to calculations of energy lost in passing through the windows and lens. The energy in the split-off portion of the beam was 10 percent of that reaching the germanium lens. The ballistic thermopile is a calorimetric device that measures the temperature rise due to absorbed

radiation. It consists of two nickel-plated cones (receiver and reference) and series connected iron-constantan thermocouples. The thermocouples are arranged so that the hot junctions are attached to the receiver cone and the cold junctions to the reference cone. Radiant energy is directed into the receiver cone where almost total absorption takes place. This results from the shape of the cone, which produces a Mendenhall wedge effect of multiple reflections. The temperature difference between receiver and reference causes an emf, which is monitored by the externally connected microvoltmeter. The peak meter reading is linearly proportional to the total input energy. Because of the high reflectivity in the cone, the surface resists the destructive effects of high peak power pulses found in laser research. Some characteristics of the ballistic thermopile are given in Table IV, Appendix B.

D. SPECTROGRAPHS

The visible radiation produced by the gas as it underwent breakdown was investigated in this study. A small spectrograph was utilized to obtain photographs of the lines present for different laser pulse energies. Light was gathered from the 90° port and focused by a 39.5 cm focal length lens onto a vertical slit. The spectrograph then produced a spectrum with a dispersion of 26.7 angstroms per millimeter from 4000 to 6000 angstroms, and resolving power of about 5 angstroms with a film. Previous work with this

spectrograph had utilized KODAK Super XX Pan Film, and had required 50 shots to produce enough light to show the spectra. For this study Polaroid type 410 high speed (ASA 10,000) film was used, held by a standard camera back. This system gave excellent results with just one shot per picture, as shown in Fig. 4.

A large, nominal three meter, folded path dual monochromator was utilized for determining the time dependence of each radiation line studied. Light from the plasma was gathered by a 23.5 cm focal length lens and focused on the entrance slit of the spectrograph. The light was split into two essentially identical paths by prisms. The monochromator had a dispersion of 4.0 angstroms per millimeter and resolving power of 0.1 angstroms. The gratings were blazed for second order green. Figure 5 is a plot of the dispersion.

The light was directed into two photomultiplier tubes, one for each channel. The tubes used were RCA 1P21 tubes with S-4 response. No cooling was necessary for work with these tubes in the visible region at the intensity levels observed. Cooling would yield better response to weaker lines, however. Additional information on the dual monochromator may be found in Ref. 25.

E. CAMERA

The high speed photographs of plasma production, expansion and dissipation were obtained with an Imacon 600 image converter camera. The camera was operated in the framing

mode only, but could be used as a streak camera. The spectral response of the system could be varied by changing tubes. In this study an S-1 response was utilized. The camera processed the radiation gathered by the optical system and produced an image on a TV screen. Permanent recording was available with Polaroid type 410 or type 47 (ASA 3000) film. Either 5, 10 or 15 frames per photograph could be selected, at frame rates up to 6×10^8 f.p.s.

The camera trigger circuit was susceptible to radio frequency interference. Triggering was produced by lightning, aircraft overhead and the Marx power supply for the laser. Since the camera was to be utilized to obtain photographs of the plasma produced by the laser beam, pre-triggering before the beam existed was a considerable problem. The problem was circumvented by utilization of a 10 meter radius copper directing mirror with the laser beam to enable placement of the gas chamber and camera at a distance from the Marx sufficient to prevent pre-triggering.

Detailed specifications of the Imacon 600 are listed in Table V, Appendix B.

IV. EXPERIMENTAL PROCEDURE

A. DETERMINATION OF LINES PRESENT

The first step in obtaining detailed spectrographic information about the breakdown was the determination of the line spectra. This was accomplished by introducing into the pressure chamber the desired amount of the particular gas to be investigated. The chamber pressure was first reduced to approximately 75 torr. Then 3 atmospheres of the gas were admitted. Again the chamber was evacuated. Then the gas was put in at the desired pressure for the experiment. This reduced to a minimum contamination from air or gases previously utilized.

Light from the plasma passed through a Pyrex window, then entered the gathering lens of the one meter spectrograph. After dispersion by the grating, the light was focused onto the Polaroid high speed film. While the film was exposed, a reference spectrum of mercury was superimposed on the spectrum from the plasma. The entire process was carried out in a dark room to eliminate excessive background.

With the mercury spectrum superimposed, there existed the probability that some lines might be hidden. This was checked by taking photographs of just the breakdown and determining by comparison which lines had been covered.

The photographic spectra were placed under a comparator microscope and the line positions were found to the nearest

micrometer. This information was then used with the Hartmann dispersion formula to determine the wavelengths of the plasma lines. The Hartmann method is described in Appendix A.

Photographs were taken of the spectra produced by varying the input energy from a fraction of a joule to several joules. This procedure yielded spectra which changed as the energy changed. Lines appeared at higher energies which had not been present at lower energies. No lines disappeared at higher energies. The continuum intensity increased at higher energies.

Once the lines to be investigated were known, it was necessary to calibrate the dual monochromator. A geissler tube containing argon was used to provide a steady source which could produce the desired response of the system to the presence of a line. The positions of the lines were tabulated, and then a mercury spectrum was produced as a standard. The Hartmann method was used again to correlate settings with wavelengths. This yielded a formula which predicted the setting to be used to locate any desired wavelength. Although argon was used to calibrate the monochromator, the formula was independent of the source of radiation.

Detailed tabulations of the spectral lines appear in Table VI, Appendix B. The table shows which lines appeared in the original spectra, which was obtained using the short

(1.5 m) focal length directing mirror, and which could be observed during the temporal investigations using the long (5 m) focal length directing mirror. Diagrams of the experimental arrangement are shown in Fig. 6. Photographs of the equipment are shown in Fig. 7.

B. TEMPORAL DEPENDENCE OF RADIATION AT VARIOUS WAVELENGTHS

Once the specific wavelengths radiated by a particular element in the plasma state were known, a detailed study of the manner in which each line changed with time could be undertaken. Preliminary information indicated that the plasma would radiate for several microseconds at an intensity sufficient to be visible to the eye [Ref. 9]. In addition, the traces were superimposed on the radiofrequency (RF) interference which was picked up by various cables and transmitted as signal to the oscilloscope. Thus, an oscilloscope trace of the variation in intensity would not show small (nanosecond) differences in lineshapes. The noise level of the uncooled photomultipliers would also prevent seeing the less intense lines. Therefore it was decided that this study would be directed towards the general, long term characteristics of the radiation. This restriction was unnecessary, as events showed that the lineshapes changed from shot to shot even on the time scale in use (1 microsecond per division). Thus, no particular lineshape could be specified for each wavelength.

The radiation was gathered, split and resolved by the optical system, and then passed via photomultipliers to a Tektronix type 555 oscilloscope, where it was displayed for photographic purposes. Comparison was accomplished by utilizing one time base as a reference, with channel "A" of the dual monochromator displayed at the same wavelength for all settings of channel "B". By ensuring the channel "A" picture remained constant in appearance, the differences between shots at various channel "B" settings could be attributed to the lines being radiated, and not to extraneous causes.

Channel "B" of the dual monochromator was set at the position calculated for the desired wavelength. If a reference arc was available it was utilized for fine tuning onto the exact center of the line. For nitrogen, however, no reference was available. This required taking numerous shots with channel "B" settings varied by a small amount each time. When the peak of the line was located, a photograph was taken. For argon and nitrogen it was possible to vary the input beam peak power, so photographs were obtained at 39KV and 45KV for argon. No significant changes were found in the argon lineshapes at different powers (with one exception at 4806Å), so nitrogen pictures were only taken at 3 atmospheres and 42KV. Helium required 8 atmospheres pressure before breakdown could be achieved with the long focal length mirror, and, consequently, only 42KV were utilized.

A plot of the more structured lineshapes observed is shown in Fig. 8. The actual shape of the lines could not be determined with certainty, since the lineshape could be varied by altering slightly the manner in which light entered the monochromator. It was possible, however, to determine that different lineshapes were present, and that their time of appearance varied.

C. PHOTOGRAPHY

The Imacon 600 high speed camera was used to provide detailed structure photographs of the plasma from the onset of breakdown to extinction of the radiation produced by the plasma. The camera was placed to view the spark through a 90° viewing port. Triggering of the camera was accomplished through delay circuitry and was initiated by the Marx generator radiation. This permitted coarse control over the start time of the pictures. Use of variable frame rates and number of frames produced picture series' with different characteristics. The choice of settings and film type was made to highlight the particular feature of the plasma that was under investigation. Photographs showing the expanding plasma are in Fig. 9.

V. DATA

A. MACROSCOPIC PLASMA PARAMETERS

The plasma produced in the gas cell was photographed by Behrens [Ref. 3] and in this study with an open face camera. In addition, a high speed framing camera was utilized to obtain details of the plasma structure. The size of the plasma as determined from photographs taken with the open face camera was on the order of 0.52 cm. However, with the high speed camera, the size of the same dimension was only 0.14 cm. The use of various apertures and filters with the high speed camera produced plasma dimensions which varied with the light intensity. Thus, it was difficult to specify the dimensions of the plasma at any time. Rather, what could be measured was the maximum extent of a curve of equal intensity. This might have been the core of the plasma, when viewed with the high speed camera; and the open face camera could have produced photographs of the light radiated from all regions into which the plasma electrons had diffused and excited atoms. It was known that the high speed camera required a greater intensity of light to produce a photograph than the open face camera, but this information could not be utilized to yield quantitative results.

The expansion rate shown by the high speed camera could be utilized only in a general manner, since it was not known to exactly what the front edge of the luminous region

corresponded. The plasma reached its maximum luminous dimensions between 450 and 530 nanoseconds after initiation. When the dimension of the plasma (0.14 cm) was divided by the time of expansion (500×10^{-9} sec), an average velocity of 3×10^{5} cm/sec resulted. This was smaller than the exponential decrease from 10^{6} cm/sec at initiation to 2×10^{5} cm/sec at 350 nanoseconds after the pulse reported by Lampis and Brown [Ref. 18]. Therefore, it was concluded that the luminous region observed on the film with the high speed camera did not include the entire plasma.

Photographs of the plasma taken with either a 1% transmission neutral density filter or no filter and an f/16 aperture on the high speed camera showed the brightest portion of the plasma to be at an angle to the incoming radiation. The angle (ϕ) was 47 degrees, measured from the assumed focal point using the laser axis as the reference line, and was directed toward the laser as appears in the sketch below:

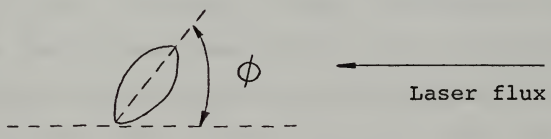

With an f/1 lens, the focussing angle measured in the same manner as ϕ above would only be 26.5 degrees. Thus, either this expansion was outside the beam, or the beam entered the chamber in a non-geometrical fashion, if the photographs

showed the actual plasma core. Insufficient time was available for further investigation of this phenomenon, and no conclusions were reached on its cause. Most probably it was a camera-produced distortion.

Measurements of the beam divergence yielded a half angle of 1.1×10^{-2} radians. This produced a focal spot size with the 2.54 cm lens of 2.32×10^{-3} cm^2, with the spot diameter equal to 0.54 mm.

B. SPECTRA OBSERVED

Photographs of the line spectra and continua emitted during breakdown provided much information on the processes involved. General features of the spectra suggested relative temperatures of the different gases, as well as demonstrating the effects of pressure broadening. Identification of the lines present yielded information on the degree of ionization attained during breakdown.

Figure 4 shows typical spectra from breakdown plasmas in argon (1 atm.), nitrogen (3 atm.) and helium (8 atm.). In Fig. 4a the nitrogen spectrum at 3 atm. corresponds to the approximate minimum pressure for breakdown with the long focal length beam directing mirror. Under these conditions the nitrogen spectrum shows a weak continuum with ionic lines superimposed. At the minimum Marx voltage for breakdown (39 KV) the continuum, if present, was so weak as to be undetectable. The ionic lines seen in Fig. 4a have widths appreciably greater than the instrument width, and

are quite weak. Helium, Fig. 4b, shows no continuum, and only two lines, which are broadened to a half width on the order of 20 to 40 angstroms. The high pressure of 8 atm. necessary for breakdown in helium is believed to be responsible for the broadening. Figures 4c and 4d show spectra in argon which were obtained at different input energies. They show an increase in brightness of both continuum and lines due only to the energy difference, since all other conditions were maintained constant. As the laser pulse energy was increased above the threshold value, the intensity and number of lines in the spectrum increased, while the background continuum also increased until at maximum voltage used in the experiment (45 KV) the line-continuum contrast disappeared.

From the fact that the continuum intensity increased in the order: He, N, Ar; and from lower to higher energy above threshold, it appeared reasonable to suggest that the electron temperatures increased in the same order.

The nitrogen line spectrum (Fig. 4a) included approximately half of the known intense lines of singly ionized atoms in the spectral range observed, and a few lines which might be tentatively assigned to the N III spectrum, although overlap with N II lines prevented definite identification. The N II lines observed were those with wavelengths of 5942, 5932, 5711, 5680, 5676, 5667, 5005, 4643, 4631, 4621, 4607, 4601, and 4447 angstroms. The N III lines in question were

at 4642/4641, 4634 and 4515 angstroms. No N I lines were observed. The absence of neutral atom lines was of interest since such lines were observed by Lampis and Brown [Ref. 18]. No plausible explanation for the absence of these lines could be found.

Lines present in the argon plasma (Fig. 4c,d) included those from neutral and singly ionized atoms. Doubly ionized atom lines might have been present at high input energies; however, the continuum and line density was such as to prevent their identification. The Ar I lines observed were those at 5651, 5534, 5496, 4888, 4876, 4522, 4511, 4334, 4300, 4272, 4266, 4259, 4201, 4191, and 4159 angstroms. The Ar II lines had wavelengths of 5145, 5142, 5062, 5017, 5009, 4965, 4933, 4880, 4848, 4806, 4765, 4736, 4727, 4658, 4610, 4590, 4579, 4545, 4426, 4401, 4380, 4371, 4348, 4331, and 4267 angstroms.

Only two lines were observed in the helium spectra (Fig. 4b). Both were neutral lines, at wavelengths of 5876 and 4471 angstroms. The presence of these lines resulted in a pinkish-blue color to the plasma, not observed with the other gases.

All lines observed in these survey spectra are designated "YES" in Table VI, column "Orig." In both the nitrogen and argon plasmas there were initially unexplained line absences - where one or two lines were not observed, while neighboring lines with wavelengths longer and shorter did

appear. Several possible explanations of this were considered. After eliminating those lines whose absence was probably due to overlap by other, observed lines, and those with transitions from different quantum levels, there still remained several unexplainably absent lines. The most puzzling question was why one or two lines of a multiplet would be missing when the others appeared. The question was tentatively resolved by first obtaining the multiplet number for each line, then determining the multiplets which exhibited line absences, and finally checking the relative line strengths calculated by Wiese [Ref. 34]. This led to an unexpected conclusion that the tabulated values for intensity [Ref. 31] were not indicative of what would be observed in a brief period. Thus, within a given multiplet, the lines which did not appear in the spectra were found to be quite weak when the calculated line strengths were used for comparison.

One additional piece of information became apparent during analysis of the spectra. The ionization potential of the singly ionized argon atom was above the calculated electron temperature. Therefore, since Ar II lines were observed, it was concluded that either the temperature determined in Section II was too low, or non-equilibrium ionization processes were involved. The lines which resulted from transitions out of the 21 eV energy level had the highest upper energy level of all lines observed in argon,

which would restrict the temperature to a value near 21 eV (if this may be used as a valid indicator of electron temperature for conditions of local thermodynamic equilibrium).

C. TIME DEPENDENCE OF RADIATION

Photographs of the photomultiplier output gave time resolved intensity measurements for each wavelength investigated. Scaled drawings of the most interesting lineshapes compared with a typical line are shown in Figure 8. In agreement with previous observations by Evtushenko [Ref. 9], the curves consisted of two separate sections. The initial portion of the curve was an intense continuum, which varied little in intensity across most of the spectrum, but was stronger at the blue end. This continuum occurred as a spike at a time coincident with the arrival of the laser pulse in the chamber; and the full width at half maximum height was about 0.4 microseconds, which agreed well with the length of the laser pulse. Thus, it was concluded that this portion of the radiation had been produced during the production and heating stages, and was believed to consist of Bremsstrahlung radiation.

Once the laser pulse had ended, the continuum dropped to a much lower intensity (Fig. 8, curve a). For argon, the ratio of continua intensity as determined by the respective peaks in the photographs (points A and B, Fig. 8) was about 5.3. Nitrogen and helium ratios were much lower, on

the order of 2.2. The second continuum was observable for 4 to 5 microseconds. This was tentatively ascribed to recombination radiation.

Approximately 2 microseconds after the initial continuum had reached maximum intensity, a second portion of the curve became evident when the monochromator was set for wavelengths emitted by the plasma. These lineshapes varied considerably from line to line (Fig. 8d,e,f) and also varied slightly from shot to shot. Argon lines presented the most clearly defined lineshapes. The Ar I lines rose to maximum intensity from 1.4 to 2.4 microseconds after the initial continuum reached its maximum, while the Ar II lines occurred from 1.4 to 2.3 microseconds after the first continuum. Generally, the lines rose to a peak in about 0.4 microseconds, then decayed exponentially with an e-folding time of about 1.5 microseconds. There were a few lines which exhibited distinctive characteristics. The Ar II line at 4806Å showed a great difference in the lineshapes at energy inputs of 0.73±.04 J and 2.55±.13 J, as shown in Fig. 8c,d. In addition, the Ar II lines at 4545, 4610, 4765 and 4880Å decayed slowly for about 1.4 microseconds on the average; and then they decayed exponentially in the same manner as the other observed lines. This delay was tentatively attributed to either a larger cross-section for excitation exhibited by these lines than by the other lines, or pumping of the upper level with energy stored in a metastable level.

No difference in the average time of maximum intensity was observed for the atomic and ionic lines, although Evtushenko [Ref. 9] reported that the ion lines occurred earlier than atomic lines. System noise was believed to have hidden such subtleties. A variation in the time of line appearance would be expected for plasmas with local thermodynamic equilibrium (LTE), wherein the excitation rates would be controlled by electron temperatures, as opposed to emission by radiative decay from recombination levels. Thus, as the plasma cools and expands, the lines arising from the highest energy levels would appear first.

D. DISCUSSION OF EXPERIMENTAL RESULTS

The data collected by photographic and spectroscopic techniques in this experiment were generally consistent with previously reported results. Consideration of the best model to describe the events observed led to that of an LSD wave during the period the laser pulse was present in the gas, and a blast wave thereafter. No effects due to reflection of the blast wave by the pressure cell back into the plasma were considered, although some perturbation of conditions might be anticipated. The reflected wave, travelling at the speed of sound in the undisturbed gas [Ref. 18] would re-enter the plasma region about 75-100 microseconds after the laser pulse subsided. This was much later than any observations of the plasma were attempted. Therefore, the

only parameters affecting the observations were gas pressure, focal spot size, laser pulse energy, laser pulse length and RF interference from the Marx power supply. Of these, only gas pressure and laser pulse energy could be varied by the experimenter. Once the minimum gas pressure which would permit breakdown was established, the only variable became laser pulse energy.

Examination of the many observed spectra for different energies (for example see Fig. 4c,d) indicated that additional input energy resulted in more intense continua (especially in the blue region of the spectrum), and caused the appearance of lines which were not apparent at lower pulse energies. That no lines radiated by highly ionized atoms were observed was in keeping with the anticipated and calculated electron temperatures, if LTE was assumed. In such a case the electron temperature would determine the maximum state of ionization at any time, and would, through collisions, establish the dominant energy levels for production of radiation at any time. The observed intensity at each wavelength investigated showed a maximum which would correspond to the point in time at which the electron temperature fell within the cross-section for excitation of the particular line if LTE was present. A plot of electron temperature vs time was produced; however, it was inconclusive. System noise appeared to destroy the anticipated consistency. The plot did show that variations in input

energy produced different delay times between the early continuum and line maxima; eg., at 0.73 J input energy the argon lines appeared approximately 0.5 microseconds earlier than when 2.56 J was utilized. However, there was no average time difference between the appearance of lines with widely varying excitation energies, while there was a great deal of time difference among lines with similar energies.

The spectra produced by gases at different pressures vividly presented the phenomenon of line broadening. At one atmosphere the lines were sharply defined and quite narrow. As the pressure was increased, the lines became less distinct. The maximum intensity decreased, while the line width increased. At eight atmospheres it was difficult to determine the center of the He I 4471Å line, which appeared only as a slight brightening over a distance corresponding to about 75 angstroms.

Most of the spectroscopic investigations conducted previously have been concerned mainly with the 5500 to 8500 anstrom portion of the radiated spectra, while only brief mention of characteristics in the 4000 to 6000 angstrom region was made. This experiment could only be conducted within the visible region from 4000 to 6000 anstroms due to the limitations of equipment and film available, but provided a base for further study of the time dependence of lines. Using the latest theories and information available, updated data could be produced to increase understanding of the laser-plasma interaction.

VI. RECOMMENDATIONS

In the course of these investigations several areas where additional work would be beneficial became apparent. Modifications to the laser, power supply shielding, high speed camera optics and dual monochromator would be required. In addition, combined use of the NPS CO_2 TEA laser and the NPS Nd-glass laser would provide additional capabilities.

The availability of a 10 meter radius of curvature copper mirror could reduce beam spread, if used as one of the cavity mirrors, rather than as a directing mirror. Then final focussing could be effected with the 3 meter radius mirror. This would increase the energy available in the beam at great distances from the laser. Using this method, the maximum useful range of the laser could be increased to about 10 meters.

Modifications to the laser electrodes are required. Arcing between the cathode and anode is subject to a threshold, where above certain input voltages, arcing is probable. During this experiment the threshold dropped from greater than 54 KV to 45 KV. This was attributed to pitting of the electrodes upon occurrence of an arc, which made subsequent arcing more probable. The aluminum utilized in construction was apparently too soft to serve adequately at the required operating voltages. Thus, a new material with

sufficient hardness should be used in construction of new electrodes.

In addition to arcing, it was observed that the laser breakdown glow was not uniform. It was most intense near the end with electrical connections from the Marx, and almost no glow was observed at the other end of the cavity. This was attributed to the poor electrical conductivity afforded by the brass rods. A copper bus with connections only at the two ends of the laser would better distribute the voltage and should produce a more uniform glow within the cavity, which would in turn increase output energy.

Throughout the experiments, RF interference from the Marx created difficulties with all electronic equipment. All cables in use acted as antennae, and the RF could be seen superimposed on whatever input signals were sent to the oscilloscope. The RF also triggered all oscilloscopes and the high speed camera. An aluminum shield constructed by Strickland [Ref. 39] to reduce the RF was only partially successful. With the shield in place, an oscilloscope could be operated within 4 feet of the Marx without triggering. Nevertheless, RF was still present. A small antenna attached to the oscilloscope was used to trigger the trace throughout the experiments. The high speed camera could be operated only if placed greater than 15 feet from the Marx. Therefore, a new shield is apparently necessary. It should be constructed of double thick, fine mesh copper wire screen and have snugly fitting corners and access doors.

Photographs obtained with the high speed camera were on a 1:1 scale with the dimensions of the object photographed. This was insufficient to identify the detailed plasma structure. Therefore a magnification system is required which would be compatible with the permanent optics. This would permit enlargement of the image when desired. If this were done, it would probably be necessary to limit its use to only the 5 and 10 frames per picture framing modes, to prevent loss of detail from overlap between one frame and the next.

Expansion of the features of the plasma observable with the present equipment could be obtained by altering the construction of the dual monochromator. If the optics were modified, infrared wavelengths from scattered radiation could be investigated. In addition, infrared detectors such as HgCdTe or PbSnTe would be required. Since obtaining a sufficient intensity of scattered radiation would be difficult with the present set-up (with most of the energy being used to produce the plasma), it would be more plausible to use the CO_2 laser to probe a plasma produced by another laser. The Nd-glass laser would produce a plasma which would exist for only a fraction of the time the CO_2 laser pulse would be present. This would permit full use of the CO_2 peak power, and scattering measurements could be obtained.

Even if no modifications to any component were to be made, there would be many areas open for future research.

Investigation of the unexplained shape of the plasma should have the highest priority. Measurements of the line intensities vs time could be improved to produce better photographs. Wavelength vs time vs position in the plasma measurements are within the capability of the present system. Since breakdown plasmas lend themselves best to spectroscopic techniques, use of the equipment and methods outlined herein should enable investigation of presently known phenomena and those yet to be discovered.

APPENDIX A

CALCULATION OF WAVELENGTH BY THE HARTMANN DISPERSION FORMULA

In general the calculation of unknown wavelengths may be made by linear interpolation between two nearby standard lines, or by use of a dispersion formula over a wide range. If many lines must be obtained, linear interpolation is rather tedious and requires that many standard lines be identified. Accuracy with any method depends on the accuracy of both standards and unknowns. Use of a dispersion formula reduces the number of lines to be identified in advance. This increases the effect of an error in measurement of the standard lines, but fewer opportunities for error are present.

The method chosen for this study is known as the Hartmann dispersion formula. It assumes the grating produces a dispersion which can be described by the equation

$$\lambda_i = A + \frac{B}{d_i - C}$$

where A, B, and C are constants to be determined for each spectrum investigated. Thus, three standard lines are required for simultaneous solution of the three equations in three unknowns. This is simplified by producing a series of simple equations, to be solved sequentially. They are

$$R = \frac{\lambda_1 - \lambda_2}{\lambda_2 - \lambda_3} \quad \frac{d_2 - d_3}{d_1 - d_2} \qquad (i)$$

$$C = \frac{R d_1 - d_3}{R - 1} \qquad (ii)$$

$$B = (\lambda_1 - \lambda_2)\left[\frac{(C - d_1)(C - d_2)}{d_2 - d_1}\right] \qquad (iii)$$

$$A = \lambda_1 + \frac{B}{C - d_1} \qquad (iv)$$

In this study, comparator readings of standard lines from the mercury spectrum were obtained and computed to provide an initial estimate of the unknown wavelengths. The more intense lines were overexposed, resulting in an apparent broadening, in order to bring out the weaker lines. This prevented an accurate determination of line position. Therefore, three lines assumed (based on the rough calculations) to be from the spectrum of interest were chosen as new standard lines. The calculations were reworked, providing an accurate formula covering the entire 400nm to 600nm spectral range investigated. A Hewlett-Packard HP-35 pocket calculator was used for the calculations. It yielded results accurate to one angstrom using only the same accuracy in the initial reference lines. In addition, it was fast and simple to operate for the numerous repetitive operations required.

Once values had been obtained for the unknown wavelengths, they were compared to tables of spectral lines [Ref. 31]. The results matched the expected source wavelengths to within 2 angstroms at all times, and they were within 1 angstrom in the majority of cases. This condition held for both the spectrometer and the dual monochromator.

APPENDIX B

TABLES

TABLE I

NPS CO_2 TEA Laser Characteristics

Energy	up to 18 joules [a]
Pulse Width	250 nanoseconds [b]
Peak Output Power	up to 25 megawatts [a]
Wavelength	10.6 micrometers
Beam Shape	square, 4.5 cm x 4.5 cm [c]
Max Input Voltage	66 kilovolts
Laser Efficiency	5% minimum

a. Only 14.4 J have been produced, with peak power of about 21 MW.
b. Considers only electron produced peak.
c. Unfocused, 75 cm from output mirror.

TABLE II

Material Properties of Germanium

Refractive Index	4.0 [a]
Transmission	47% [a]
Specific Heat	0.074 cal/gm-°C
Density	5.33 gm/cm^3
Thermal Expansion Coeff.	6.1 x 10^{-6}/°C
Thermal Conductivity	0.14 cal/cm-sec-°C

a. At 10.6 micrometers.

TABLE III

ORIEL Photon Drag Detector

Response Time	less than 1 nanosecond
Responsivity	0.18 mV/KW [a]
Output Resistance	50 ohms
Operating Temperature	room temperature

a. At 10.6 micrometers

TABLE IV

HADRON Ballistic Thermopile

Ballistic Time Constant	50 seconds
Equivalent Noise Level	300 microjoules
Max Energy Input	1000 joules
Max Power Input	1×10^9 watts
Sensitivity	45 microvolts/joule
Output Impedance	100 Ohms
Measurement error	less than 5%

TABLE V

IMACON 600 Camera

Spectral Sensitivity	S1
Framing Speed	7.5×10^7 to 6×10^8 f.p.s
Photon Gain:	
Without Image Intensifier	50
With Image Intensifier	1×10^6
Longest Time Span/Photograph	200 nanoseconds
Time Resolution	3 picoseconds
No. of Frames	5, 10, 15
Spatial Resolution	3 to 5 line pairs/mm
Streak Writing Speed	0.1 to 60 mm/ns

TABLE VI

Plasma Line Radiation

λ, Å [a]	I_B [b]	E_B, eV [c]	Orig. [d]	I_o [e]	Time [f]	I_t [g]	J [i]
			NITROGEN				
			N I (E_i = 14.5 eV)				
5564.37	9	13.99	NO	- [h]	-	-	5/2-7/2
5560.37	9	14.00	NO	-	-	-	7/2-9/2
4935.03	10	13.20	NO	-	-	-	3/2-1/2
4151.46	12	13.32	NO	-	-	-	5/2-3/2
4109.96	12	13.70	NO	-	-	-	3/2-5/2
4099.95	9	13.70	NO	-	-	-	1/2-3/2
			N II (E_i = 29.61 eV)				
5941.65	12	23.24	YES	5	NO	-	2-3
5931.78	11	23.24	YES	4	NO	-	1-2
5710.77	10	20.64	YES	4	NO	-	2-2
5686.21	10	20.64	NO	-	-	-	1-1
5679.56	14	20.66	YES	9	YES	5	2-3
5676.02	11	20.64	YES	9	YES	3	0-1
5666.63	12	20.66	YES	8	YES	5	1-2
5010.62	10	20.94	NO	-	-	-	1-1
5007.33	11	23.41	NO	-	-	-	1-2
5005.15	14	23.14	YES	10	YES	7	3-4
5001.48	12	23.13	NO	-	-	-	2-3
5001.14	11	23.12	NO	-	-	-	1-2
4994.36	10	23.42	NO	-	-	-	1-1
4643.09	11	21.15	YES	3	YES	7	2-1
4630.54	14	21.15	YES	5	YES	9	2-2
4621.39	10	21.15	YES	3	YES	4	1-0
4607.16	10	21.15	YES	3	YES	6	0-1
4601.48	11	21.16	YES	3	YES	3	1-2
4447.03	12	23.19	YES	9	YES	7	1-2
4041.31	11	26.21	NO	-	YES	3	4-5
			N III (E_i = 47.44 eV)				
4641.90	7	33.13	YES	2	YES	7	3/2-3/2
4640.64	10	33.13	YES	2	YES	7	3/2-5/2
4634.16	8	33.13	YES	2	YES	3	1/2-3/2
4514.89	7	38.40	YES	2	NO	-	5/2-7/2
4379.09	10	42.54	NO	-	-	-	5/2,7/2-7/2,9/2
4103.37	9	30.46	NO	-	-	-	1/2-1/2
4097.31	10	30.46	NO	-	-	-	1/2-3/2

TABLE VI
(continued)

λ, Å	I_B	E_B, eV	Orig.	I_o	Time	I_t	J
			HELIUM				
			He I (E_i = 24.59 eV)				
5875.62	7500	23.07	YES	10	YES	1	2,1-3,2,1
4471.48	1000	23.73	YES	4	YES	3	2,1-3,2,1
			He II (E_i = 54.41 eV)				
5411.52	50	53.30	NO	-	NO	-	7/2,5/2-9/2,7/2
4685.68	300	51.01	NO	-	NO	-	5/2,3/2-7/2,5/2
			ARGON				
			Ar I (E_i = 15.76 eV)				
5650.71	1500	15.10	YES	2	YES	2	1-0
5606.73	500	15.12	NO	-	-	-	1-1
5558.70	500	15.14	NO	-	-	-	1-2
5534.45	60	15.54	YES	1	NO	-	2-1
5495.88	1000	15.33	YES	2	NO	-	3-4
5187.75	800	15.30	NO	-	NO	-	1-2
5162.29	500	15.31	NO	-	-	-	1-1
4887.95	200	15.44	YES	1	YES	8	1-1
4876.26	200	15.45	YES	1	YES	6	1-2
4702.32	1200	14.46	NO	-	-	-	1-1
4628.44	1000	14.51	NO	-	-	-	1-2
4596.10	1000	14.52	NO	-	-	-	1-1
4522.32	800	14.46	YES	1	YES	2	0-1
4510.73	1000	14.58	YES	1	NO	-	1-0
4345.17	1000	14.66	NO	-	-	-	1-1
4335.34	800	14.69	NO	-	-	-	1-1
4333.56	1000	14.69	YES	3	YES	7	1-2
4300.10	1200	14.51	YES	1	YES	4	1-2
4272.17	1200	14.52	YES	1	NO	-	1-1
4266.29	1200	14.53	YES	1	YES	8	1-2
4259.36	1200	14.74	YES	1	NO	-	1-0
4251.19	800	14.46	NO	-	-	-	2-1
4200.68	1200	14.50	YES	1	NO	-	2-3
4198.32	1200	14.58	NO	-	-	-	1-0
4191.03	1200	14.66	YES	1	NO	-	0-1
4190.71	600	14.51	NO	-	-	-	2-2
4181.88	1000	14.69	NO	-	-	-	0-1
4164.18	1000	14.52	NO	-	-	-	2-1
4158.59	1200	14.53	YES	1	YES	3	2-2
4044.42	1200	14.69	NO	-	-	-	1-2

TABLE VI
(continued)

λ, Å	I_b	E_B, eV	Orig.	I_o	Time	I_t	J
			Ar II (E_i = 27.63 eV)				
5537.29	5	25.67	NO	-	-	-	3/2-5/2
5145.32	25	19.55	YES	1	YES	6	3/2-5/2
5141.79	20	21.14	YES	3	YES	8	5/2-7/2
5062.04	30	19.26	YES	3	YES	7	1/2-3/2
5017.16	20	21.13	YES	2	YES	8	3/2-5/2
5009.33	30	19.22	YES	3	YES	9	3/2-5/2
4965.07	25	19.76	YES	3	YES	10	1/2-3/2
4933.21	25	19.26	YES	5	YES	9	3/2-3/2
4879.86	30	19.68	YES	10	YES	11	3/2-5/2
4847.82	25	19.30	YES	5	YES	10	3/2-1/2
4806.02	35	19.22	YES	12	YES	18	5/2-5/2
4764.86	25	19.87	YES	4	YES	10	1/2-3/2
4735.91	25	19.26	YES	4	YES	9	5/2-3/2
4726.86	25	19.76	YES	3	YES	8	3/2-3/2
4657.89	25	19.80	YES	1	-	-	3/2-1/2
4609.56	25	21.14	YES	6	YES	10	5/2-7/2
4589.90	25	21.13	YES	6	YES	10	3/2-5/2
4579.35	25	19.97	YES	6	YES	9	1/2-1/2
4545.05	25	19.87	YES	8	YES	8	3/2-3/2
4430.19	20	19.61	NO	-	-	-	1/2-3/2
4426.01	25	19.55	YES	8	YES	13	3/2-5/2
4400.99	20	19.22	YES	5	YES	10	7/2-5/2
4379.67	20	19.64	YES	4	YES	8	1/2-1/2
4371.33	20	19.26	YES	3	-	-	5/2-3/2
4348.06	50	19.49	YES	5	-	-	5/2-7/2
4331.20	25	19.61	YES	3	YES	10	3/2-3/2
4277.52	20	21.35	NO	-	-	-	5/2-3/2
4266.53	25	19.55	YES	1	YES	8	5/2-5/2
4228.16	20	19.68	NO	-	-	-	3/2-5/2
4131.73	15	21.43	NO	-	-	-	3/2-1/2
4103.91	20	22.51	NO	-	-	-	7/2-5/2
4072.01	25	21.50	NO	-	-	-	5/2-5/2
4013.86	25	19.49	NO	-	-	-	7/2-7/2

a. Wavelength, from standard tables.[1]
b. Intensity, from standard tables.
c. Upper energy level of the transition.
d. Did the line appear in the original spectrum?
e. Arbitrary relative value from 1-15 assigned by visual inspection of the original spectra.

---

1. The tables used for this information were compiled by Striganov and Sventitskii [Ref. 31] from various sources, and were published as received, without producing a uniform intensity scale for the separate portions.

TABLE VI
(continued)

f. Did the line appear in the time resolved spectrum?
g. Arbitrary relative value from 1-20 assigned by using maximum intensity on voltage scale in use for the time resolved spectra.
h. Indicates no measurement attempted.
i. Angular momentum quantum number.

TABLE VII

Electron Temperatures [a]

Gas	Input Energy			
	0.73J	0.91J	1.69J	2.56J
Ar (1 atm)	13 [b]	18	40	65
N_2 (3 atm)	1.6	3	9	16
He (8 atm)	1.9	3	8	13

a. For each gas, at all energy levels, the level of ionization was considered equivalent to that for complete ionization at one atmosphere pressure; i.e., for each gas 8.27×10^{16} atoms were assumed ionized. The dissociation energy for all the nitrogen molecules was 1.36×10^{18} eV, and was considered in the calculations.
b. Temperatures in eV.

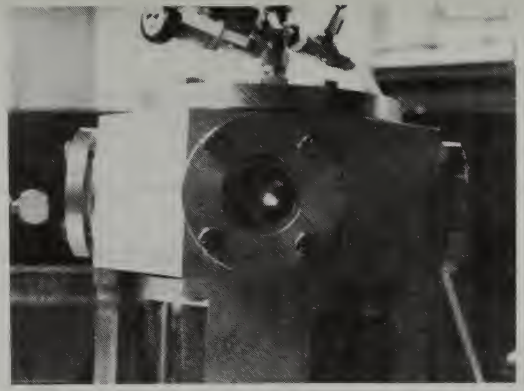

(a)

(a) Argon plasma at 1 atm.
Laser energy 0.73 J

Light flux

(b) Closeup of argon plasma.
Pressure 1 atm.
Laser energy 0.73 J

Light flux

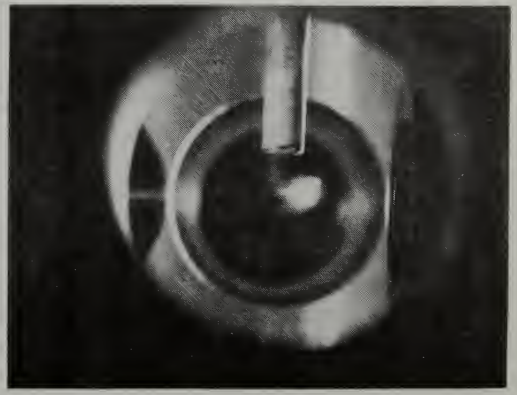

(b)

Figure 1
Typical Spark Photographs

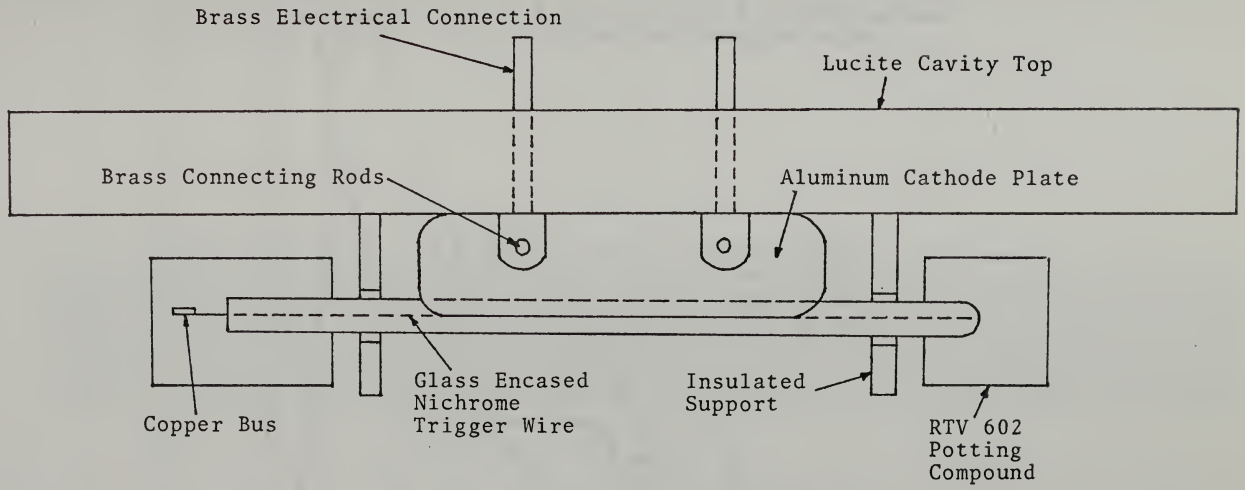

Figure 2
CO_2 TEA Laser Cathode

(Not to Scale)

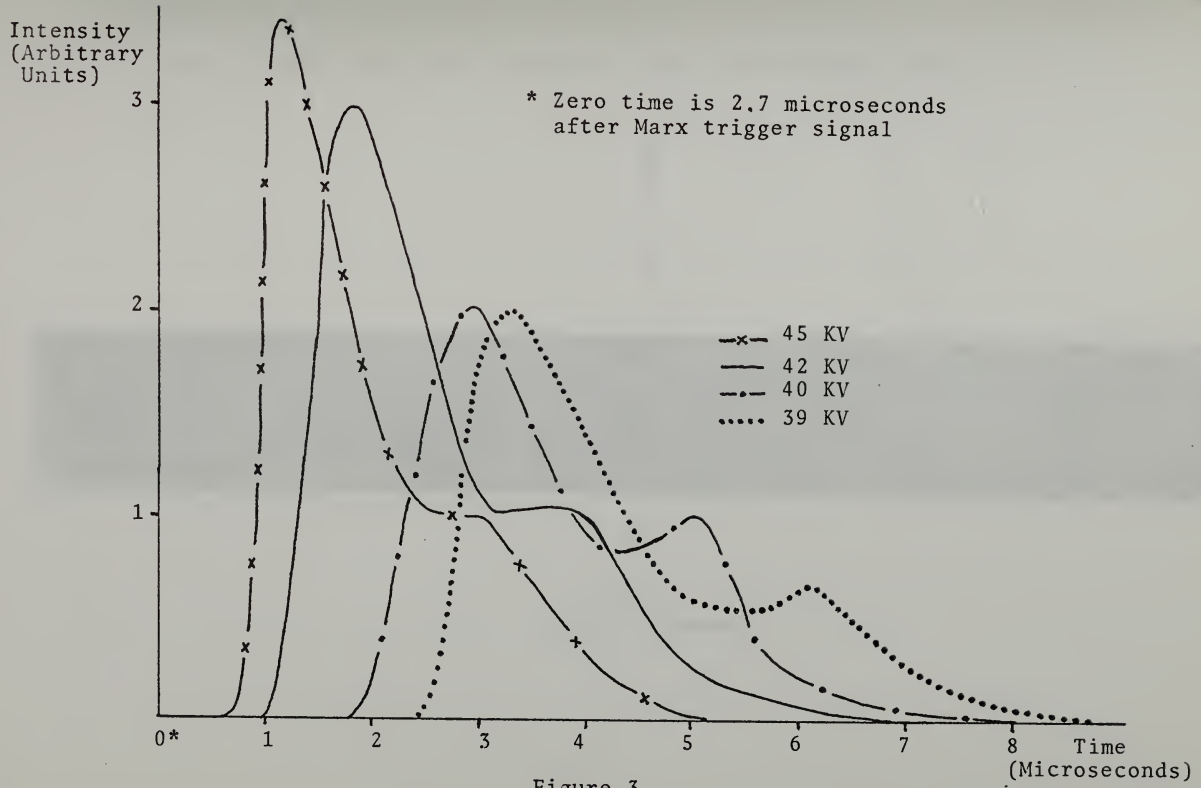

Figure 3
Laser Pulse Shapes

(a) Nitrogen spectrum: Pressure 3 atm.; Laser energy 2.56 J

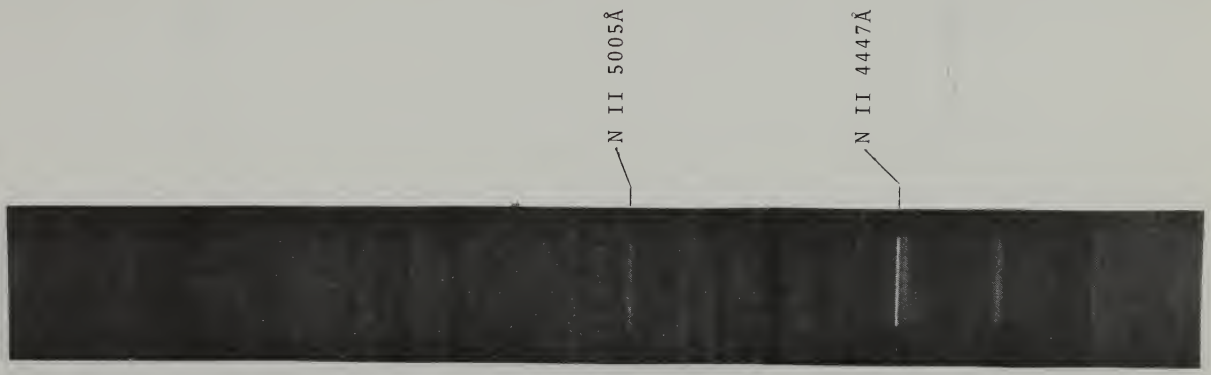

(a)

Figure 4
Typical Spectra

(b) Helium spectrum: Pressure 8 atm.; Laser energy 2.56 J

Fig. 4(b)

(c) Argon spectrum: Pressure 1 atm.; Laser energy 0.73 J

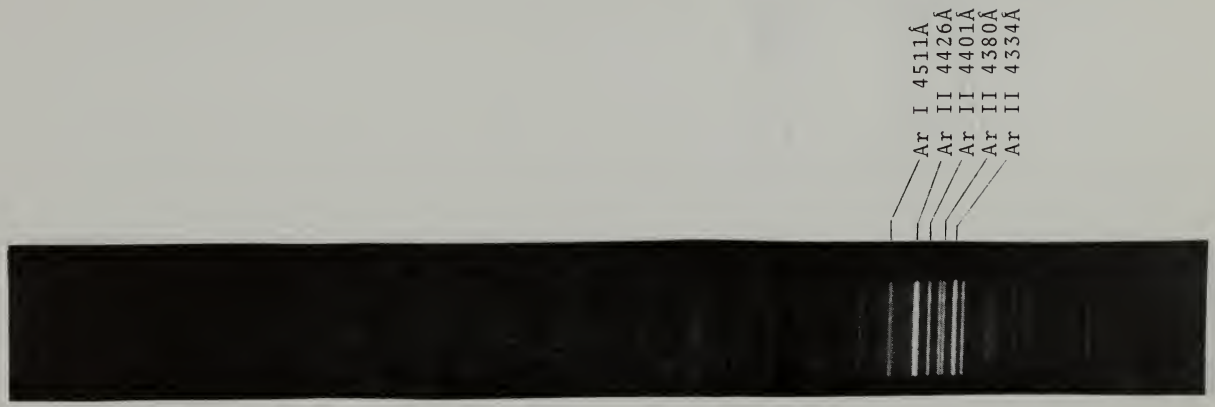

Fig. 4(c)

(d) Argon spectrum: Pressure 1 atm.; Laser energy 1.69 J

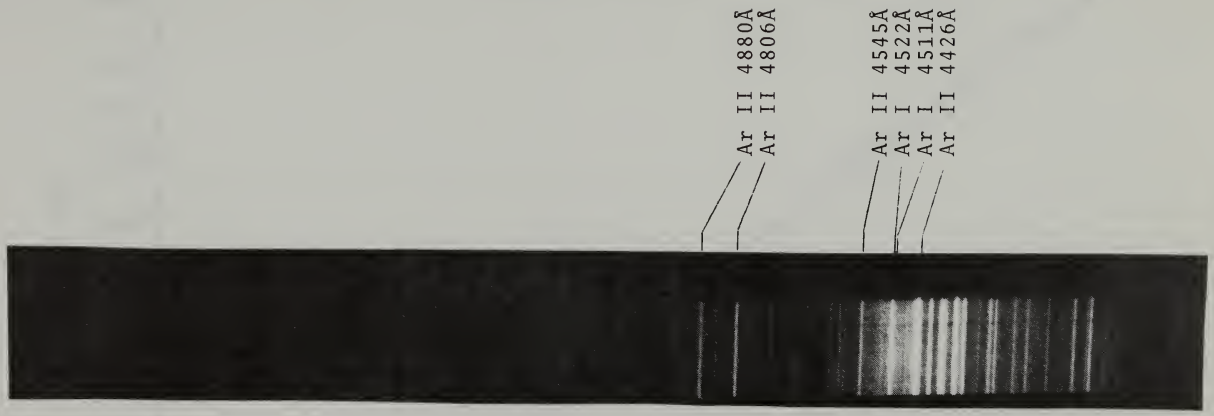

Fig. 4(d)

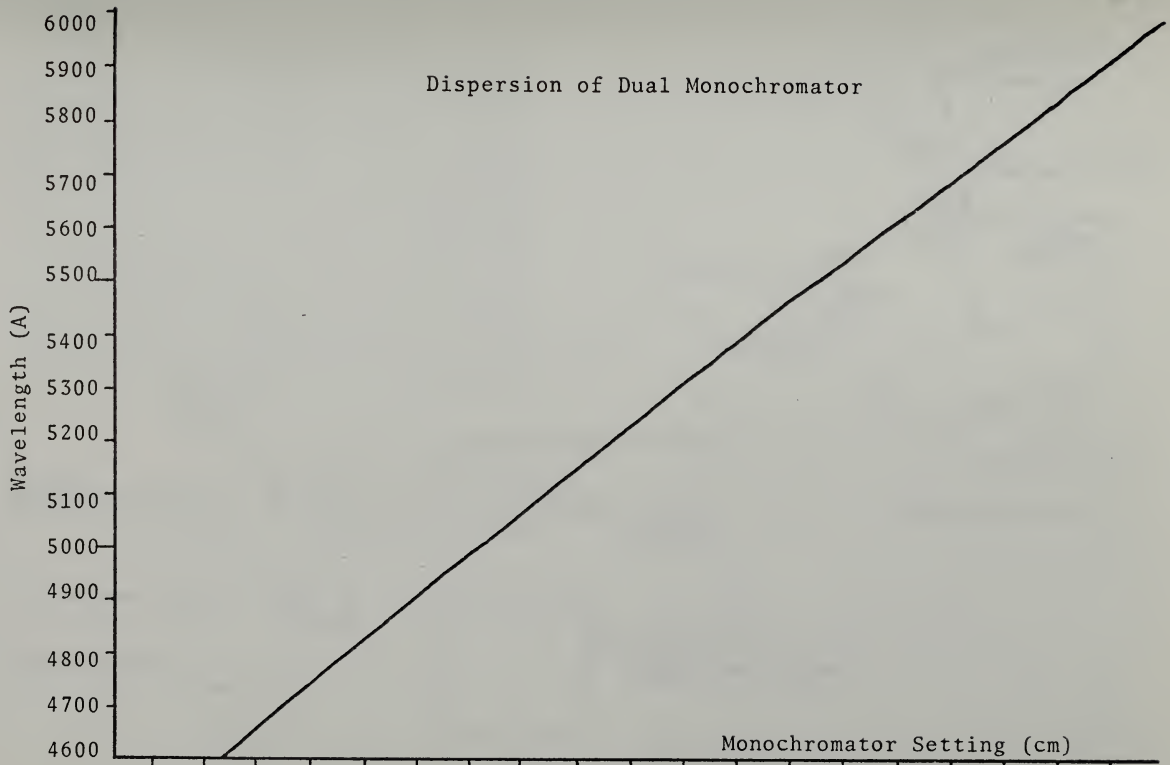
Dispersion of Dual Monochromator
Wavelength (A)
6000
5900
5800
5700
5600
5500
5400
5300
5200
5100
5000
4900
4800
4700
4600
Monochromator Setting (cm)
210
230
260
290

Figure 5

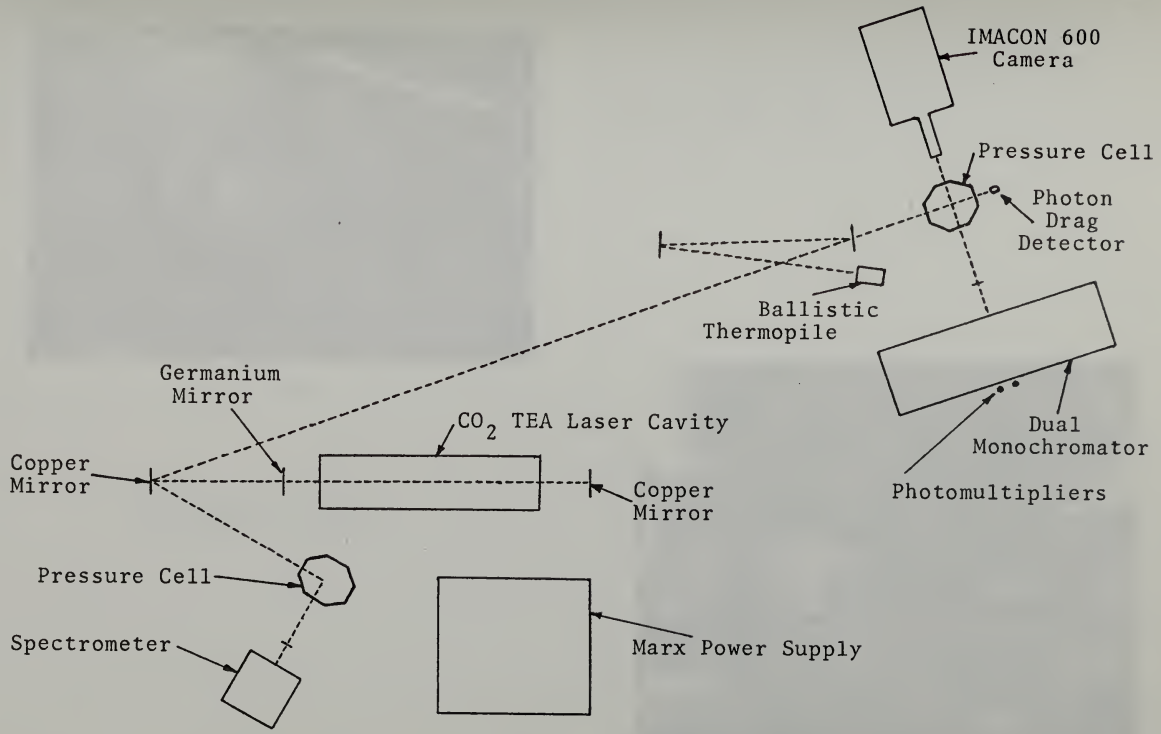

Figure 6
Diagram of
Experimental Arrangements

(a) CO_2 TEA Laser

(a)

(b) Pressure Cell and
Dual Monochromator

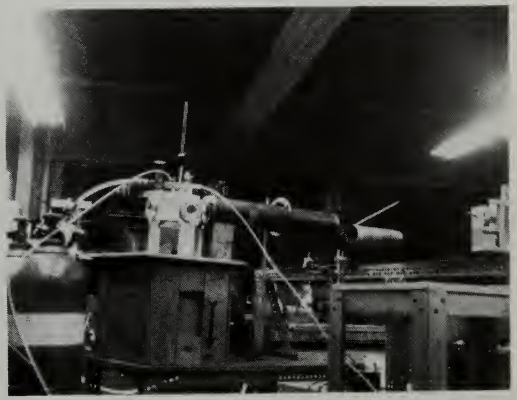

(b)

Figure 7
Photographs of Equipment

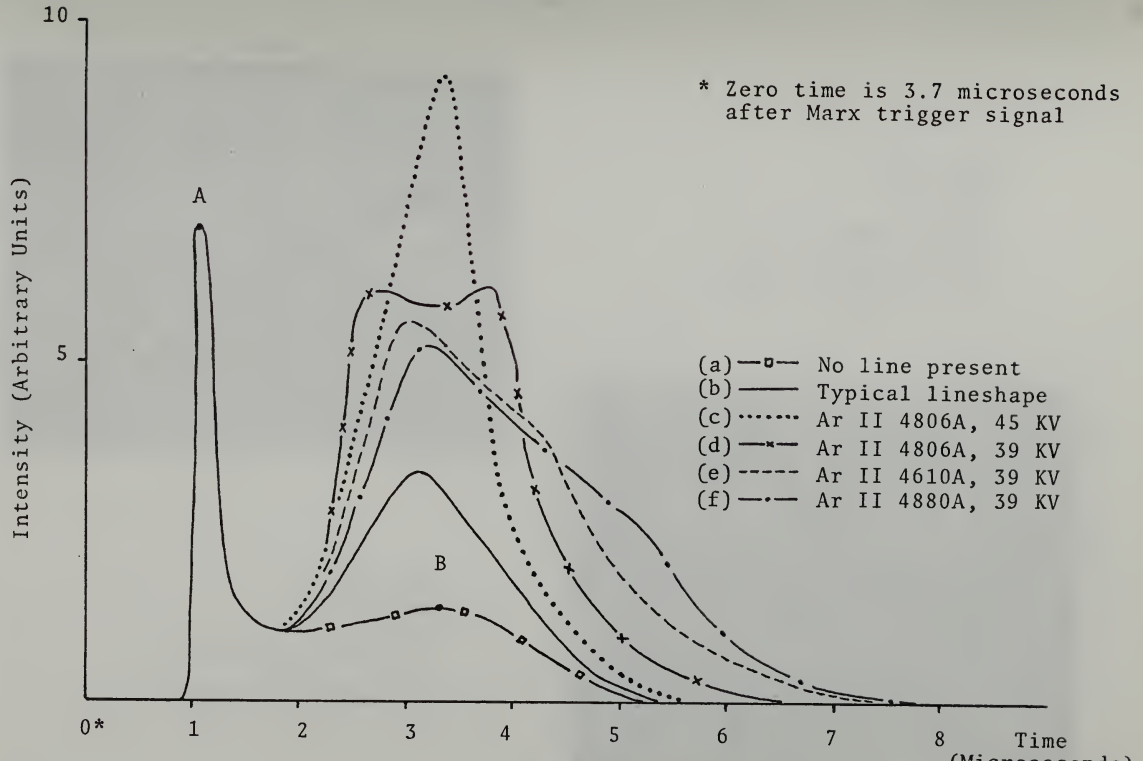

Figure 8
Argon Plasma Lineshapes

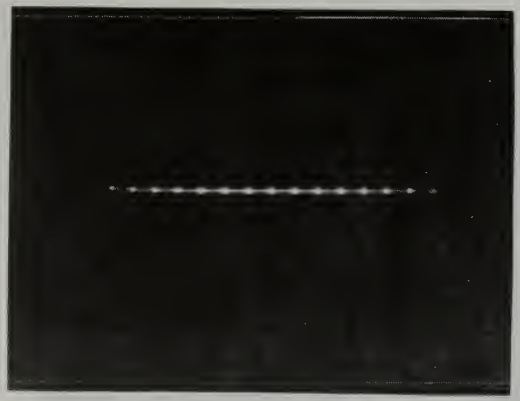

(a)

(a) Argon plasma, 1 atm., 1.69 J
15 frames per picture
7.5x10 f.p.s.
Scale approximately 1:1
f/11.2
No filter
Film type 47

(b) Argon plasma, 1 atm., 1.69 J
10 frames per picture
7.5x10 f.p.s.
Scale approximately 1:1
f/11.2
No filter
Film type 47

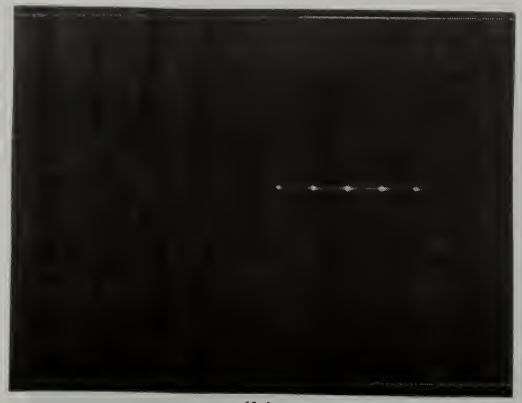

(b)

Figure 9
Photographs of an Expanding Plasma

(c)

(c) Argon plasma, 1 atm., 1.69 J
15 frames per picture
7.5x10 f.p.s.
Scale approximately 1:1
f/4.0
1% filter
Film type 410

(d)

(d) Argon plasma, 1 atm., 1.69 J
15 frames per picture
7.5x10 f.p.s.
Scale approximately 1:1
f/3.6
1% filter
Film type 410

Figure 9
continued

BIBLIOGRAPHY

1. Bassett, W. F., Investigation and Operation of a Carbon Dioxide TEA Laser, Master's Thesis, Naval Postgraduate School, Monterey, Ca., 1973.

2. Bates, D. R. et al., "Recombination Between Electrons and Atomic Ions', Proc. Royal Soc., London, A267, p. 297 (1962).

3. Behrens, P., Breakdown Phenomena in Rare and in Molecular Gases Using Pulsed Carbon Dioxide Laser Radiation, Master's Thesis, Naval Postgraduate School, Monterey, Ca., 1974.

4. Braerman, W. F. et al., "Spectroscopic Studies of a Laser-Produced Plasma in Helium", Journal of Applied Physics, v. 40, p. 2549, 1969.

5. Browne, P. F., "Mechanism of Gas Breakdown By Lasers", Proc. Phys. Soc., v. 86, p. 1323, 1965.

6. Brown, R. T. and Smith, D. C., "Laser-Induced Gas Breakdown in the Presence of Preionization", Applied Physics Letters, v. 22, no. 5, p. 245, 1973.

7. Daiber, J. W. and Thompson, J. W., "Laser Driven Detonation Waves in Gases", Physics of Fluids, v. 10, no. 6, p. 1162, 1967.

8. Daiber, J. W. and Winans, J. G., "Radiation from Laser-Heated Plasmas in Nitrogen and Argon", Journal of the Optical Society of America, v. 58, no. 1, 1968.

9. Evtushenko, T. P. et al., "Spectroscopic Studies of a Laser Spark", Soviet Physics - Tech. Phys., v. 11, p. 1126, 1967.

10. Fabre, E. and Stenz, C., "CO_2 Laser Beam Absorption by a Dense Plasma", Physical Review Letters, v. 32, no. 15, p. 823, 1974.

11. Griem, H. R., Plasma Spectroscopy, McGraw-Hill, N.Y., 1964.

12. Hacker, M. P. et al., "Low Pressure Gas Breakdown with CO_2 Laser Radiation", Applied Physics Letters, v. 23, no. 7, p. 392, 1973.

13. Huddlestone, R. H. and Leonard, S. L., Plasma Diagnostic Techniques, Academic Press, N.Y., 1965.

14. Ireland, C. L. M. and Grey-Morgan, C., "Gas Breakdown by a Short Laser Pulse", Journal of Physics D: Applied Physics, London, v. 6, p. 720, 1973.

15. Korobkin, V. V. et al., "Investigation of the Air 'Spark' Produced by Focused Laser Radiation", Soviet Physics, JETP, v. 26, no. 1, p. 79, 1968.

16. Korobkin, V. V. and Alcock, A. J., "Self-Focusing Effects Associated with Laser-Induced Air Breakdown", Physical Review Letters, v. 21, no. 20, p. 1433, 1968.

17. Kunze, H. J. in Plasma Diagnostics, Ed: Lochte-Holtgreven, North Holland Publ., Amsterdam, 1968.

18. Lampis, G. and Brown, S. C., "Afterglow Measurements of a Laser Breakdown Plasma", Physics of Fluids, v. 11, no. 6, 1968.

19. Litvak, M. M. and Edwards, D. F., "Electron Recombination in Laser Produced Hydrogen Plasma", Journal of Applied Physics, v. 37, p. 4462, 1966.

20. Mandel'shtam, S. L. et al., Soviet Physics JETP, v. 22, p. 91, 1966.

21. Morgan, F. et al., "Laser Beam Induced Breakdown in Helium and Argon", Journal of Physics D: Applied Physics, v. 4, p. 225, 1971.

22. Mulser, P. et al., "Plasma Production by Laser", Physics Reports, v. 6C, no. 3, 1973.

23. Offenberger, A. A. et al., "Plasma Diagnostics Using CO_2 Laser Absorption and Interferometry", Journal of Applied Physics, v. 42, p. 574, 1972.

24. Offenberger, A. A. and Burnett, N. H., "CO_2 Laser-Induced Gas Breakdown in Hydrogen", Journal of Applied Physics, v. 43, no. 12, p. 4977, 1972.

25. Orlicki, G. A., Spectroscopic Diagnostics of a Nitrogen Plasma, Master's Thesis, Naval Postgraduate School, Monterey, Ca., 1968.

26. Raizer, Y. P., "Heating of a Gas by a Powerful Light Pulse", Soviet Physics, JETP, v. 21, no. 5, p. 1009, 1965.

27. Raizer, Y. P., "Breakdown and Heating of Gases Under the Influence of a Laser Beam", Soviet Physics, USPEKHI, v. 8, p. 650, 1966.

28. Ramsden, S. A. and Davies, E. R., "Radiation Scattered from the Plasma Produced by a Focused Ruby Laser Beam", Physical Review Letters, v. 13, no. 7, 1964.

29. Ready, J. F. Effects of High-Power Laser Radiation, Academic Press, N.Y., 1971.

30. Spitzer, L. Jr., Physics of Fully Ionized Gases, Interscience Publ., N.Y., 1962.

31. Striganov, A. R. and Sventitskii, N. S., Tables of Spectral Lines of Neutral and Ionized Atoms, IFI Plenum, N.Y., 1968.

32. Strickland, H. W., Modifications to and Investigation of Arc Formation in a Carbon Dioxide TEA Laser System, Master's Thesis, Naval Postgraduate School, Monterey, Ca., 1974.

33. Zel'dovich, Y. B. and Raizer, Y. P., Physics of Shock Waves and High Temperature Thermodynamic Phenomena, Ed: Hayes and Probstein, Academic Press, N.Y., 1966.

34. Wiese, W. L., Smith, M. W. and Miles, B. M., Atomic Transition Probabilities, Vol. 2, NSRDS-NDS22, 1969.

INITIAL DISTRIBUTION LIST

		No. Copies
1.	Library, Code 0212 Naval Postgraduate School Monterey, California 93940	2
2.	Professor K. E. Woehler, Code 61 Chairman, Department of Physics and Chemistry Naval Postgraduate School Monterey, California 93940	2
3.	Assoc. Professor A. W. Cooper, Code 61 Cr Department of Physics and Chemistry Naval Postgraduate School Monterey, California 93940	4
4.	Lt. R. W. Stevenson, USN 11 Eleventh Avenue Haddon Heights, New Jersey 08035	1
5.	Assoc. Professor F. Schwirzke, Code 61 Sw Department of Physics and Chemistry Naval Postgraduate School Monterey, California 93940	2

161387

Thesis
S71435 Stevenson
c.1 Spectroscopic examina-
tion of carbon dioxide
laser produced gas
breakdown.